University of New Hampshire

Analysis of Wingtips Devices for Marine Applications

University of New Hampshire
TECH 797 Undergraduate Ocean Research Projects
Fall 2016 - Spring 2017
28 April 2017

Team Members

Jamison Couture – Mechanical Engineer

Alexander Larson – Mechanical Engineer

Cole Matthews – Mechanical Engineer

Project Advisors

Dr. Martin Wosnik

Dr. Ivaylo Nedyalkov

Sea Grant New Hampshire

Acknowledgements

We would like to give a special thanks to the following project contributors, without which this project would not been possible:

- Dr. Ivaylo Nedyalkov
- Dr. Martin Wosnik
- Gavin Hess
- Aleksandra Wojtowicz
- Timothy Barrett
- Michael Cook

This work is the result of research sponsored in part by the New Hampshire Sea Grant College Program through NOAA grant # NA10OAR4170082, and the UNH Marine Program.

Abstract

Wingtip devices, such as aircraft winglets, are designed to enhance the overall wing/blade performance by diminishing the tip vortices. In underwater marine applications, wingtip devices can also mitigate cavitation. Cavitation is the formation of vapor in a liquid due to low pressure – rather than high temperature. Cavitation may cause significant problems for underwater turbines or propellers because it can greatly reduce their performance and lifespan.

This project aims at defining when cavitation occurs in terms of its flow parameters: cavitation number and Reynold's number. Experiments were done using the High-Speed Cavitation Tunnel (HiCaT) in the Jere A. Chase Ocean Engineering building at the University of New Hampshire. Numerical analysis was done using an open source computational fluid dynamics (CFD) software, OpenFOAM. Both methods investigated a plain wingtip and a wingtip device at multiple angles of attack and flow speeds to understand and quantify how wingtip devices affect the behavior of cavitation. It was found that a wingtip device causes cavitation to occur at lower pressures for the same angle of attack.

Table of Contents

List of Tables

List of Figures

1 Introduction & Project Motivation

Cavitation is a known phenomenon on wings and wingtips subject to liquid flows. It occurs when the pressure drop across the wing is large enough to vaporize the fluid. This vapor is then entrained in the vortex shedding and can stay as a vapor far downstream of the wing.

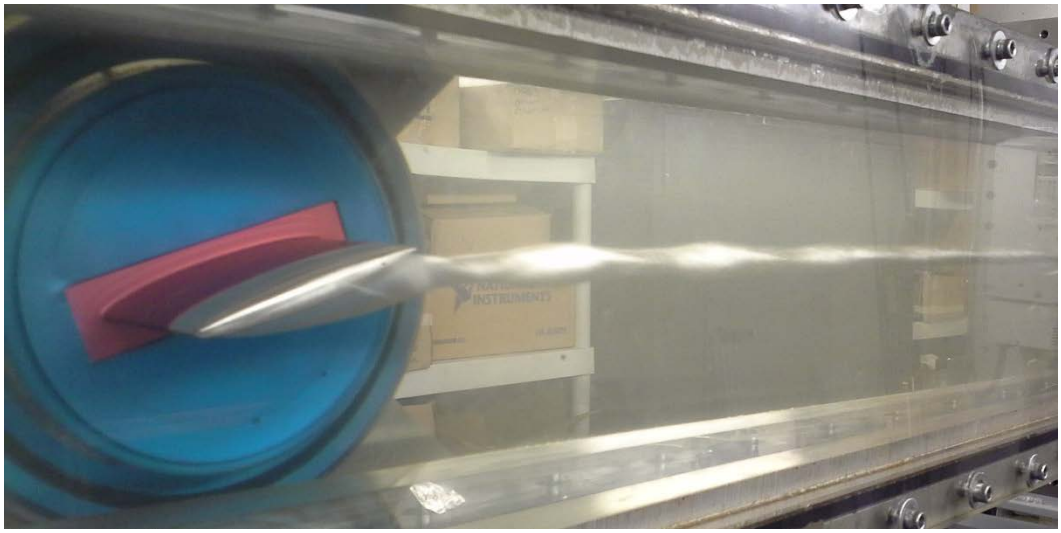

Figure 1: Cavitation trail of the End Cap wingtip in the High-Speed Cavitation Tunnel at the University of New Hampshire

Cavitation is well understood and can be accurately predicted using 2D simulations for the wing span; however, it is not well defined for the region surrounding the wingtip other than for elliptically loaded devices. Cavitation can be detrimental to underwater devices, i.e. turbines and propellers because it acts as mini-explosions when colliding with bodies downstream. Due to the delayed desinence of cavitation, if there are devices downstream of the cavitating body they become susceptible to its harmful effects. Cavitation forming on or hitting the surface of an object can cause the object to erode. With the recent surge in ocean tidal energy, this work is extremely relevant because understanding cavitation will allow companies, such as ORPC in Maine or Verdant Power in New York, to design their blades to minimize cavitation. Consequently, increasing a turbine's lifespan and saving the industry money.

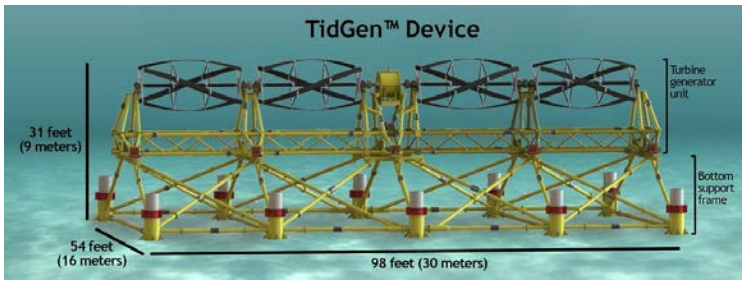

Figure 2: ORPC's turbine in crossflow

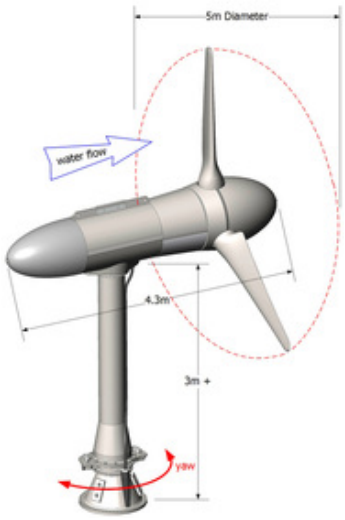

Figure 3: Verdant axial flow tidal turbine.

This project aims at defining the inception and desinence parameters for different wingtips across a broad spectrum of angles of attack, Reynolds numbers, and cavitation numbers. To properly identify the inception and desinence parameters, theoretical, numerical, and experimental analysis will be run on different wingtip designs.

- Theoretical Analysis:

  Investigation of past research and publications regarding the phenomena of cavitation and wingtip devices, and the fluid dynamics of the situation to understand the governing equations.

- Numerical Analysis:

  Comparison of various wingtip designs through numerical analysis using the open source computational fluid dynamics (CFD) software OpenFOAM.

- Experimental Analysis:

  Testing of the wingtip devices in the High-Speed Cavitation Tunnel (HiCaT) at Jere A. Chase Ocean Engineering building to observe and record their inception and dissonance parameters.

2 Theory

Cavitation is studied in terms of a non-dimensional, rescaled value called the cavitation number (σ). The cavitation number rescales the pressure differential between the static pressure of the fluid flow and the vapor pressure of the liquid that the flow is made of. This differential is divided by the flow's dynamic pressure.

$$\sigma = \frac{p_r - p_v}{\frac{1}{2}\rho U^2} \tag{1}$$

where p_r is the static pressure of the flow, p_v is the vapor pressure of the fluid, ρ is the density of the fluid, and U is the mean freestream velocity of the fluid. It is important the vapor pressure of the fluid is included in the cavitation number because it reflects the rate of vaporization of the fluid, and it is important to note that this factor is temperature dependent.

To understand the behavior of a wingtip and eventually derive a function for cavitation inception, three more nondimensionalized terms need to be brought forward: Reynold's Number (Re_c), coefficient of lift (C_L), and coefficient of drag (C_D). Reynolds Number is a force ratio of inertial forces over viscous forces describing whether a flow is laminar or turbulent. Knowing if a flow is laminar or turbulent is important because the boundary layer of the wing changes along with its performance and behavior.

$$Re_C = \frac{Uc}{\nu} \tag{2}$$

where c is the chord length of the foil and ν is the viscosity of the fluid.

It is important to characterize the coefficient of lift and drag for the wing because these define its efficiency. These values are the rescaled force ratio of the lift or drag force, respectively, verse the dynamic pressure on the lifting area.

$$C_L = \frac{F_L}{\frac{1}{2}\rho cLU^2} \tag{3}$$

$$C_D = \frac{F_D}{\frac{1}{2}\rho cLU^2} \tag{4}$$

where F_L and F_D are the lift and drag forces, respectively, and L is the span of the foil.

As discussed by Dr. Arndt in *Cavitation in Vortical Fl*ows, the inception of tip vortex cavitation for an elliptically loaded foil follows the relation:

$$\sigma = KC_L^2 Re_c^{0.04} \tag{5}$$

where K is a nondimensional value ranging from 0.035 to 0.073 depending on the study. It is important to note the coefficient of lift is squared in Equation 5 because this reflects the strength of the tip vortex. [2]

To investigated the inception of cavitation two different wingtips were used. The End Cap wingtip was chosen as a control because it is the simplest version of a wingtip and offers a baseline for cavitation inception. The General wingtip was then chosen because this design can be seen in many different modern applications. It theoretically delays cavitation because the end geometry hinders the strength of the tip vortex.

Figure 4: Investigated wingtips, from left to right, End Cap and The General.

3 Analytical Analysis of Lift and Drag Coefficients

When considering any experiment or design, it is desirable to have an analytical basis, serving as a method for verification of computational and experimental results. In the sense of this project, analytical results are possible and well known for the study of lift-drag performance and cavitation inception curves for elliptically loaded wingtips and foils. The End Cap wingtip was analyzed in this study because it is the only wingtip available that is elliptically loaded. The cavitation analytical approach is discussed in ***Theory***. As for the lift and drag analysis, known equations were used as discussed below to reach analytical results for the End Cap wingtip device.

For a true representation of the lift-drag analysis for the wingtip device, the tip vortex effects for a finite wingspan must be investigated to correct the 2-D lift and drag coefficients. The presence of wingtips introduces variations in the spanwise flow across the wing section, and depending on the device, leads to non-elliptical loading. The wingtip vortices induce a generally downward velocity directly behind the wing, called downwash. The downwash velocity is added to the free stream velocity, resulting in an apparent flow velocity tilted by a small angle (induced angle of attack). This effect reduces the effective angle of attack the wing is operates at. The result is that a finite wing must operate at a greater angle of attack than expected from 2-D foil analysis to achieve the same lift-drag performance.

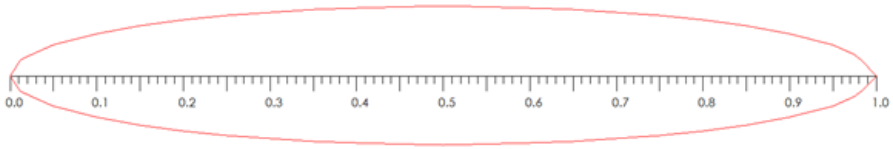

Figure 5: Non-Dimensional Elliptical Airfoil Geometry

As the End Cap wingtip device does not follow a NACA or well described shape, it was desired to discretize the foil to allow for analytical analysis. *Figure 5* shows the nondimensionalization of the End Cap foil. 2-D polars for the End Cap wingtip were calculated in XFOIL, to provide a basis for a 3-D correction factor to be applied.

To allow for easy comparison to experimental data, the airfoil of the End Cap was analyzed from -3 to 12 degrees of angle of attack, and at a Reynolds number of 395,000 (6). This value is slightly below that of the experimental data, but it has been found in previous studies that deviations of Reynold's number for the flows over the tested wingtip devices does not result in significant shifts in the coefficients of lift and drag.

$$Re = \frac{U_\infty c}{\nu} \tag{6}$$

Table 1: Wing Geometry

Span (S)	0.095 m
Chord (c)	0.079 m
Aspect Ratio	1.20

As previously stated, the 3-D wing theory used in this analytical study [6] considers an elliptical loading across the span (S) of the finite wing. This distribution is caused by span-wise circulation. The distribution for this circulation is given in (7).

$$\Gamma(y) = \Gamma_0 \sqrt{1 - \left(\frac{y}{S}\right)^2} \tag{7}$$

$$\text{Where: } \Gamma_0 = \frac{4\,L}{\rho_{water}\, V_\infty\, S\, \pi} \tag{8}$$

To consider finite aspects of the wingtip device, the downwash velocity must be known to calculate the induced angle of attack. It is known from previous studies that for elliptically loaded foils, the downwash velocity (w) is uniform over the wingspan for any given angle of attack (9).

$$w(\alpha) = \frac{\Gamma_0}{2S} \tag{9}$$

Once the downwash velocity was calculated, the induced angle of attack (α_i) could be approximated (10). Due to the known ratio between the downwash velocity and the freestream flow velocity, $w \gg V_\infty$, the small angle approximation can be used to calculate the induced angle of attack.

$$\alpha_i = \frac{w}{V_\infty} \tag{10}$$

As stated before, the induced angle of attack acts to reduce the geometric angle of attack. With this known, the effective angle of attack was calculated by taking the difference between geometric and induced angles (11).

$$\alpha_{eff} = \alpha - \alpha_i \tag{11}$$

Since there is no twist present in the foil across its span, α_{eff} can be applied to the entire foil. With this known, all lift (L) and drag (D) vectors were rotated by α_{eff} in a counter clockwise manner. *Figure 6* illustrates the geometry of this rotation.

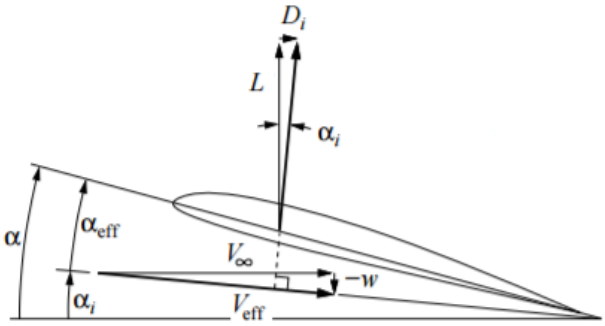

Figure 6: Geometry Changes to Angle of Attack and Induced Drag [Anderson]

From this new angle of attack for the system, the induced drag can then be calculated using (12). This calculated drag was then used to calculate the induced drag coefficient (13).

$$D_i = \alpha_i L \tag{12}$$

$$c_{D,i} = \frac{D_i}{\frac{1}{2}\rho_{water} V_\infty^2 S} \tag{13}$$

The total drag coefficient was calculated by summing the 2-D foil drag coefficient and the induced drag coefficient.

From previous analytical studies, the analytical lift coefficient is a function of the foil aspect ratio and the induced angle of attack (14).

$$C_L = -\alpha_i \, \pi \, AR \tag{14}$$

With the coefficients of lift and drag calculated and corrected, the C_L/C_D ratio (a general measure of foil performance) was calculated to allow for comparison to experimental results over a range of geometric angles of attack from 0°-12°.

4 Numerical Analysis

In order to have the most complete analysis possible, numerical analysis was performed in addition to the cavitation experiments conducted in the HiCaT. This analysis was performed using the open-source computational fluid dynamics (CFD) program OpenFOAM. This program is powerful, has a wide range of post-processing capabilities and is free to use. The simulations modeled the test section of the HiCaT with a model of a foil protruding from the side in a similar fashion to the experiments.

To perform a simulation there was a specific sequence of steps that was followed. First, an .stl file was created from the SolidWorks model of the desired foil. This file was then placed in the correct folder in the OpenFOAM file structure so the program could recognize it when it created the simulation geometry. Next, the test section geometry was defined by creating a 3D model and defining how many finite volumes each coordinate direction was to be divided into using the **blockMesh** command. For example, if the setting (10 8 6) was used the program would divide the geometry into 10 volumes in the x-direction, 8 volumes in the y-direction, and 6 volumes in the z-direction for a total of 480 finite volumes. To optimize the performance of OpenFOAM the aspect ratio of each finite volume should be approximately one.

Once the test section geometry had been meshed, the foil geometry was extracted from the .stl file using the **surfaceFeatureExtract** command and merged with the test section geometry using a tool known as Snappy Hex Mesh. This tool was used by executing the **snappyHexMesh** command. Snappy Hex Mesh is an extremely powerful tool included with OpenFOAM that saves the user countless hours trying to create complicated meshes on their own. It searches through the block mesh until it finds a finite volume where the block mesh and the foil mesh coincide. When it finds such a volume it divides that volume into eight smaller volumes. The number of times each volume is decomposed depends on the level of refinement that was defined before the function is executed. These simulations used a refinement level of 5, meaning that each volume where the two meshes intersected was decomposed into 8^5 volumes. All of these volumes are not kept, however. Once the decomposition is complete, the function goes through and deletes the volumes that do not contain part of the foil boundary. Once the volumes have been decomposed and the erroneous volumes removed, the remaining mesh is “snapped” to the geometry surface. This means that the vertices of the remaining volumes are moved so they land on the geometry surface. This is a huge aid to the user because it quickly refines the mesh and matches it to the geometry surface. Without this aid the meshing process would take many times longer because the user would have to define all of the complicated vertex locations in order to have the geometry defined fully enough to have useful results.

After the mesh was fully defined, the **simpleFoam** command was used to execute the simpleFoam solver and the simulation was started. As the solver iterated through the mesh it solved for various flow parameters such as velocity and pressure. After the solver was completed, the results were viewed and analyzed using ParaView, another open-source program that contains powerful analysis tools such as the ability

to create streamlines and look at properties across a plane perpendicular to the flow. These capabilities are illustrated in *Figures 7* and *8*.

It is worth noting that both the snappyHexMesh and simpleFoam processes were ran in parallel. This was because both processes are extremely computationally intensive and if they were run on a single processor the simpleFoam solver alone could take upwards of 50 hours to finish running. However, the core-simulator computing station located in the Chase laboratory has 8 processors and by splitting the work between each processor reduced the run-time to approximately 18 hours. This was then reduced to approximately 5 hours by shortening the length of the test section model. To decompose the mesh, the **decomposePar** command was used. This command splits the mesh evenly amongst each processor to increase the efficiency of the task. Once the process was complete the **reconstructPar** command was used to put the decomposed mesh back together. Once the mesh was reconstructed it could then be analyzed in ParaView.

Unfortunately, since cavitation is the instantaneous formation of vapor in a liquid there are no computing processes that can handle the instant change in properties of a simulation parameter. This means that, currently, it is impossible to numerically model cavitation. However, pressure can easily be calculated and a correlation could be drawn between the pressure data and the cavitation data collected through experiments. By performing many simulations, it may be possible to bridge the gaps between experimental data points, effectively providing a smooth curve from which cavitation can be predicted.

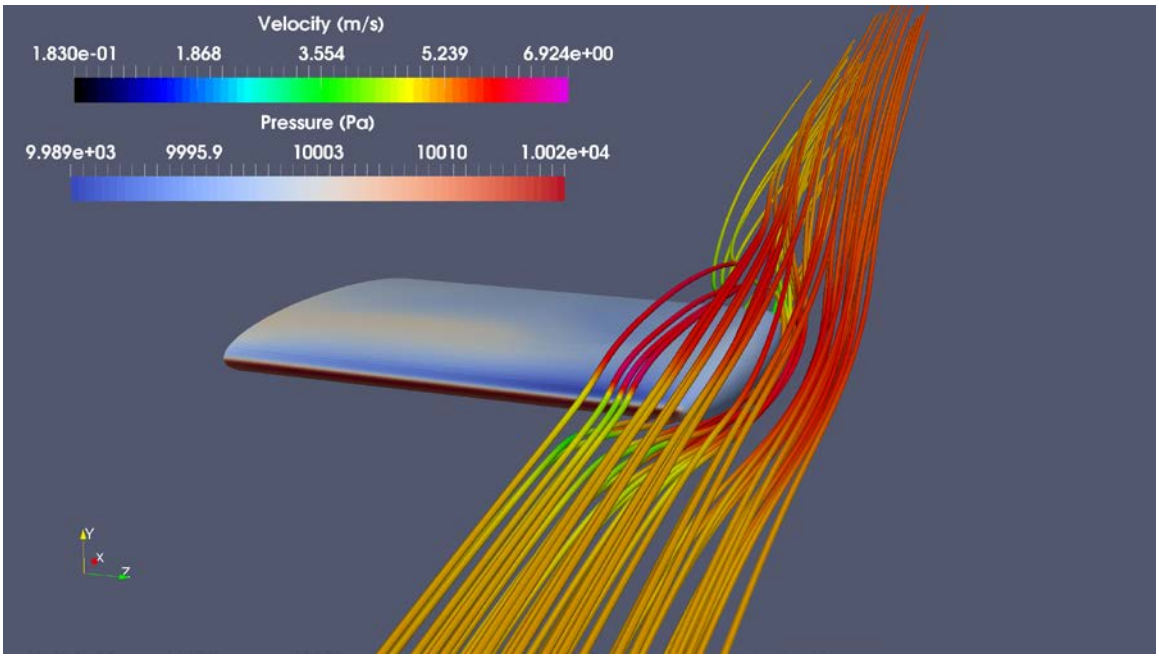

Figure 7. OpenFOAM simulation of the endcap at an angle of attack of 12 degrees and a flow velocity of 5 m/s.

Figure 7 depicts the results of an OpenFOAM simulation of the End Cap. The streamlines show the general motion of the flow and along the streamlines is a velocity gradient. As the flow passes over the wingtip it curls slightly in a counter-

clockwise direction and increases velocity. Additionally, along the profile of the tip a pressure gradient is displayed. As expected, in areas of high velocity, such as the edge of the wingtip, the pressure is also very low. Since cavitation cannot be directly modeled numerically it can be approximated using the pressure data. Since the pressure is very low at the edge of the wing and the flow is beginning to rotate it can be inferred that this is the place where the cavitation trail will first attach to the wing. This can be seen in Figure 16.

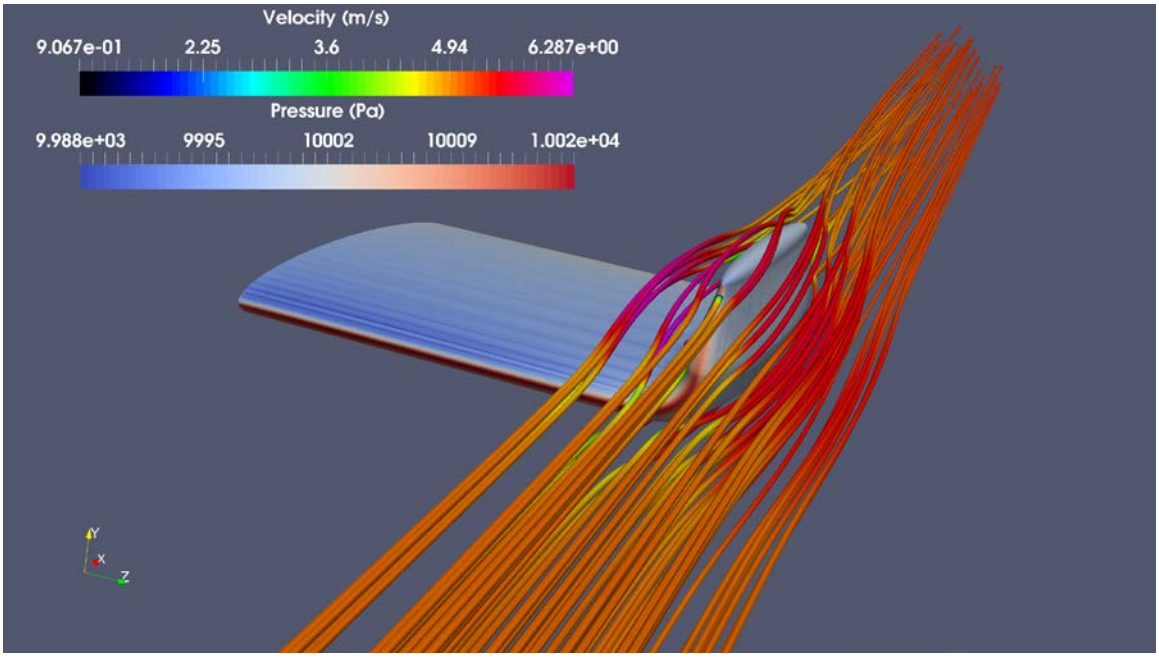

Figure 8. OpenFOAM simulation of the general tip at an angle of attack of six degrees and a flow velocity of 5 m/s.

This figure shows the behavior of the flow as it passes over the General tip. Similar to the endcap the flow is beginning to curl in a counter-clockwise direction. This is consistent with the observations gathered during the experimental testing. Also, the flow is at its highest velocity as it passes over the tip of the vertical edge of the general tip. This, combined with the fact that the pressure is low there, indicates that this is the location where the cavitation trail will connect. Again, this is consistent with experimental observations and can be seen in Figure 17.

5 Experimental Analysis

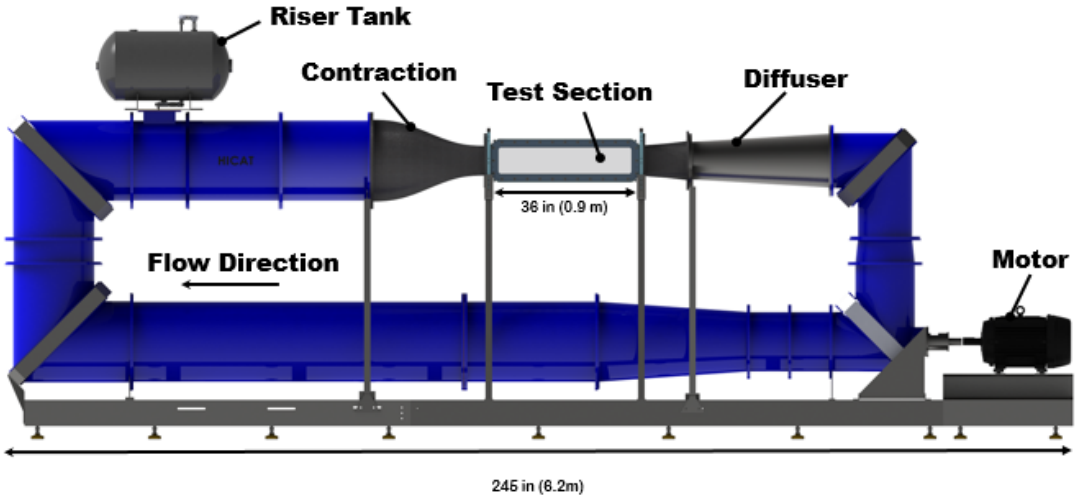

Figure 9: Diagram of HiCaT

All experimental testing was done in the HiCaT at UNH. The experiment was uses a force balance to measure the lift and drag forces of the wingtips which is calibrated with every individual experiment. An electric motor spins a propeller to move the water at a desired velocity. The static pressure of the system is controlled by a pressure transducer, an air compressor, and a vacuum. The HiCaT can maintain absolute pressures of 25 kPa to 180 kPa and reach speeds between 1.3 m/s and 13 m/s.

5.1 Static Calibration

When preparing for an experiment the first step was to calibrate the force balance. This was done in a very systematic way to ensure the procedure was standardized and could be repeated easily each time. The process was as follows:

1. Remove acrylic window opposite the force balance by first taking out the three bolts on the vertical flange of the upstream end of the test section. Once these three bolts have been removed, loosen the socket cap screws securing the window in the test section. After the window has been removed, cover it with ice to freeze it so it can be reinserted later.

2. Remove the smaller acrylic window on the bottom of the test section, making sure to first remove the singular bolt at the downstream end of the test section and then removing the socket cap screws. It is important to keep these screws separate from the screws that are used for the side window. Similar to the side window, freeze this window as well so it can be reinserted easily.

3. Next, attach the pulley to the test section making sure to line up the center pin of the pulley with the fourth bolt hole from the downstream end of the test section. Note: this is only for drag calibrations; if calibrating for lift, the pulley is not used at all. Make sure to place the rubber shims between the clamping metal pieces and the test section to ensure that the test section does not become damaged.

4. Loosen the four bolts securing the foil holder to the force balance, taking care not to hit the drag plats with a wrench. Once all four bolts are loosened slide the foil holder out of the force balance.

5. If there is a wingtip in the holder, remove the four screws securing it to the holder. Be careful, as the wingtip, extender, and base will become separate pieces as the two middle screws are removed. Once the foil holder is empty, attach the calibration block to the holder using four short screws. These screws should be the same length as the two used for the outer two screw holes.

6. Slide the foil holder back in the force balance. Using a digital level, measure the angle of the test section relative to the ground and record this angle. Using the same level, make the calibration block parallel to the test section and tighten the four bolts on the force balance. Once the bolts are secure, recheck the calibration block to make sure it is still parallel to the test section.

Figure 10: Electronic level setup with calibration block

7. Next, place the handle onto the end of the foil holder that is protruding from the back of the force balance. Using the same digital level from the previous step, measure the angle of the handle relative to the ground and record this measurement. This is important because as the angle of attack is changed this slight variation needs to be included to make sure the foil is at the correct angle of attack.

8. If calibrating for drag, place the hook in the hole at the back of the calibration block so that it is parallel with the flow direction. If calibrating for lift, place the hook in the hole on the perpendicular surface so that it is vertical with the hook pointing down and out of the cavity where the bottom window used to be.

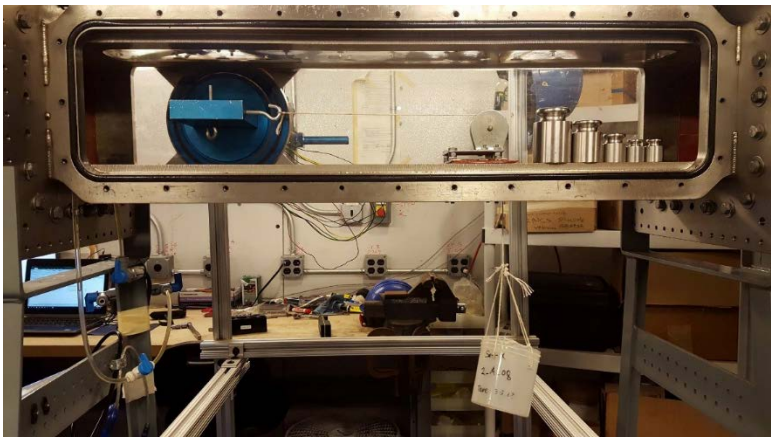

Figure 11: Drag calibration setup

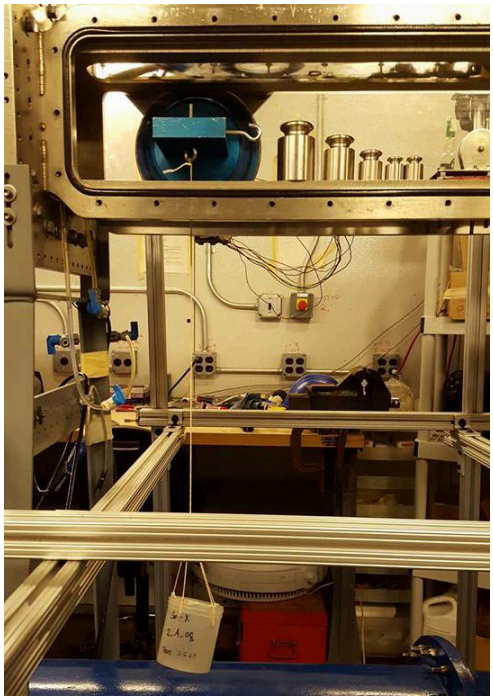

Figure 12: Lift calibration setup

9. Attach the bucket to the hook and let it swing until it is still.

10. Open the **Calibration_Balance.vi** LabView file and make sure there is a zero in the run number box and the mass is set to zero grams. Make sure you have enough masses to calibrate from zero to 1600 grams in increments of 200 grams.

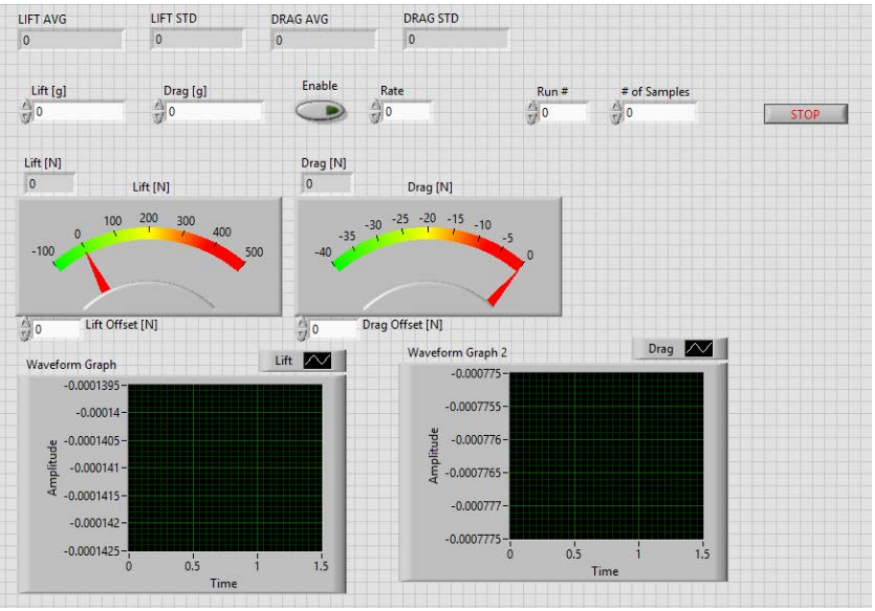

Figure 13: LabVIEW calibration VI

11. Once the bucket is still, run the VI and click enable. Wait for approximately 30 seconds for the program to collect data.

12. After 30 seconds has passed, unclick the enable button. Place 200 grams into the bucket and make sure it is still.

13. Click the enable button and wait 30 seconds.

14. Repeat steps 12 and 13 until there are 1600 grams in the bucket and 30 seconds of data has been collected.

15. Calibrate for the other force. For example, if lift was calibrated first, switch to drag by attaching the pulley and switching the position of hook. Vice versa, if drag was calibrated first, switch the set up to calibrate for lift by changing the position of the hook to vertical.

16. Once both lift and drag have been calibrated, the four bolts holding the foil holder can be loosened and the holder removed.

17. The calibration block should be removed from the holder and replaced with the desired foil.

18. Replace the bottom acrylic window and replace all the socket cap screws and bolts. Make sure the window is fully seated before tightening any screws.

5.2 Experimental Methods

Once the force balance calibration is complete the cavitation experiment procedure is as follows:

1. Mount the desired wingtip, foil extension if needed, and mounting base to force balance shaft with required O-rings. Apply Dow Corning High Vacuum Grease to all the O-rings before assembly and anti-seize to last ¼" of all screws.

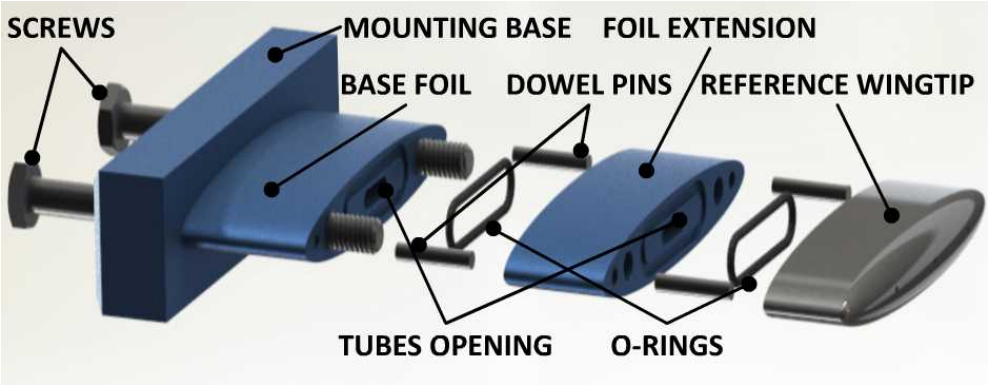

Figure 14: Wingtip assembly

2. Install the force balance assembly in the force balance, set to the first desired angle of attack (AoA), tighten the four force balance bolts, and recheck the AoA.

3. Install the side acrylic window following the same process as the bottom window described in step 18in the static calibration procedure. Once all screws and bolts are replaced and tight, commence the filling of the tunnel.

4. Open the HiCaT_Testing.vi LabVIEW file and fill in the required information:

   a. Test Piece
   b. Span and Chord
   c. Sensitivities for Drag and Lift forces
   d. Angle of Attack and Water Temperature
   e. Motor Speed in RPM
   f. Run #
   g. Desired Pressure

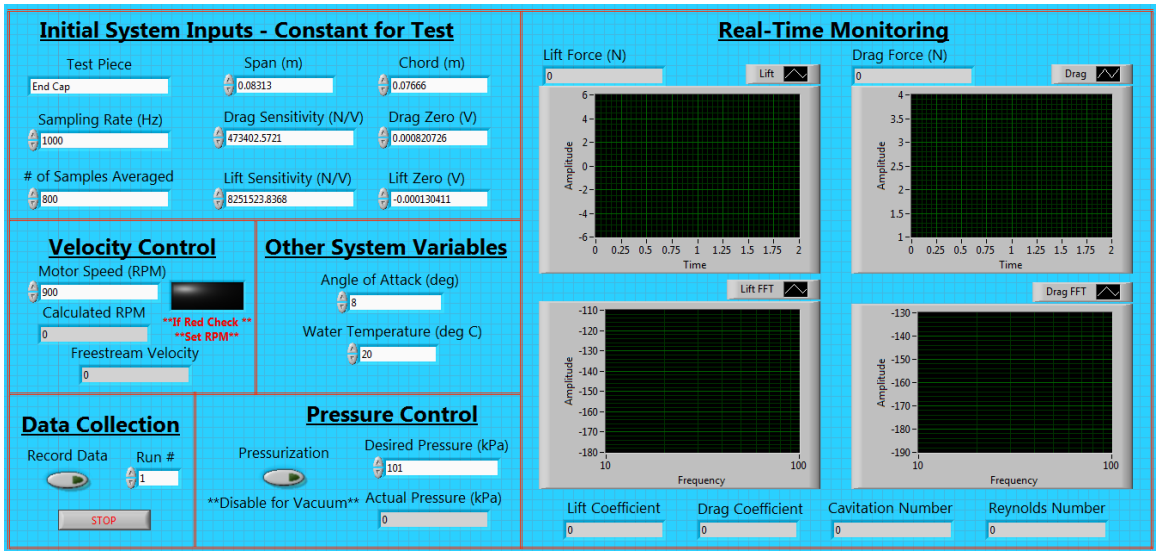

Figure 15: Cavitation experiment LabVIEW VI

5. When the HiCaT is filled to the marked line on the riser tank and before the motor has been turned on, run the LabVIEW file opened and adjust the Lift and Drag Zeroes so the Lift and Drag Force readout is as close to zero as possible.

6. Turn on the motor, set to 250 RPM, and set the desired pressure to 110 kPa. Now purge the HiCaT using water lines before the contraction section and after the diffuser until these are running clear, meaning there are no bubbles coming out of the lines.

7. Set the motor speed to 700 RPM and run here for two minutes. Then drop back down to 250 RPM and repeat step 6 to fully purge the system. Add water back into the HiCaT so the water level is back at the mark on the riser tank.

8. The HiCaT is now ready for the first experiment. Set the pressure to 170 kPa and slowly ramp up to the desired motor speed. Pause every 100 RPM for 1 minute and when the motor speed is within 100 RPM of the desired increase by 20 RPM at a time pausing for 1 minute in between. This process prevents shock cavitation from happening. If the flow is clear, proceed with the cavitation investigation. If not, stop the motor, wait till the flow stops, and then try again increasing the motor speed at smaller increments.

9. The first case to find is possible cavitation inception. Decrease the pressure slowly and be careful of overshoot. Possible cavitation inception is defined when the vapor trail is first visible with an LED flashlight. A two-person confirmation system is used to verify if cavitation inception has been found at the tip. If both people agree it has, then increase run number and collect the data. If one person does not, decrease the pressure until both agree.

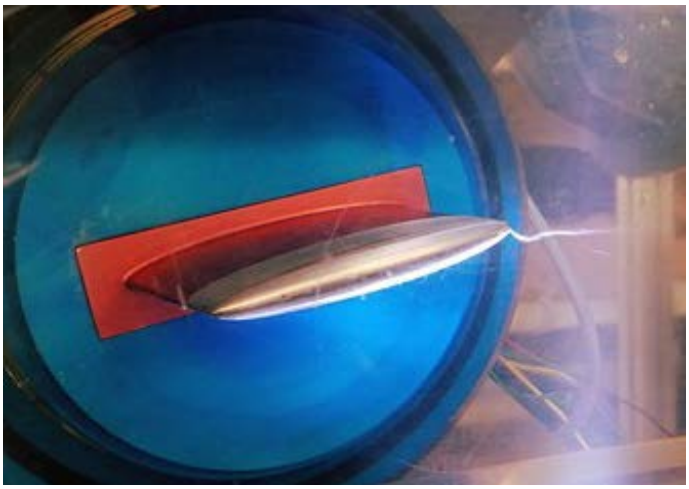

Figure 16: Possible cavitation inception example

10. The next case to test for is definite cavitation. This occurs when a cavitation trail is visible to the naked eye, without the help of a flashlight. The two-person confirmation criterion still applies. Decrease pressure slowly and be careful of overshoot. Before data is recorded ensure correct run number.

Figure 17: Definite cavitation

11. Now slowly increase pressure to test for possible cavitation dessinence. This occurs when the vapor trail begins to flicker in and out of sight to the naked eye. Dessinence does not occur instantaneously so pause every 5 kPa for 2 to 5 minutes and watch the vapor trail for flickering. The two-person confirmation criterion still applies. Before data is recorded ensure correct run number.

12. The next test point it definite cavitation dessinence. This occurs when no vapor trail can be seen with the flashlight. Increase pressure slowly and pause every 5 kPa for 2 to 5 minutes and what to see if the vapor trail disappears. The two-person

confirmation criterion still applies. Before data is recorded ensure correct run number.

13. After one full data set of cavitation inception and dessinence it may be necessary to purge, especially if the HiCaT was brought far below atmospheric pressure. Repeat steps 6 and 7 for this procedure.

14. Once the HiCaT is purged and clear, repeat steps 8 – 12 for the next data set. It is important to note that angle of attack is the most uncertain measurement in this experiment. Therefore, all motor speeds and cavitation points were recorded before the angle of attack was changed.

15. When testing is done, drain the HiCaT, remove side and bottom window, and disassemble the drag balance shaft assembly.

6 Results and Discussion

6.1 Endcap Lift and Drag Analysis: Experimental vs Analytical

From the analytical analysis, the theoretical corrections to the 2-D airfoil data produced mixed results. The 2-D airfoil polars were calculated in XFOIL using the coordinates given Appendix A. The XFOIL code did not converge at all angles of attack, and so a 3rd order polynomial fit was applied to the data for smoothing and curve creation (*Figure 18*).

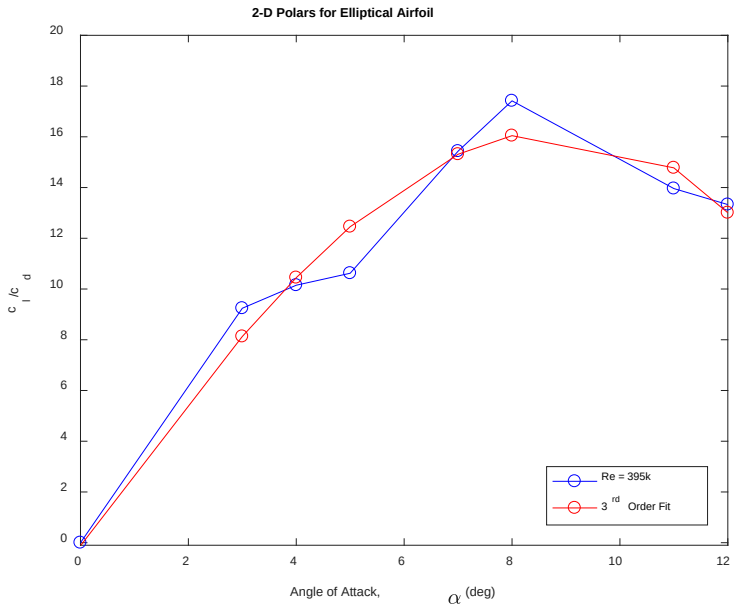

Figure 18: XFOIL Polar Output and 3rd Order Fit of Data

From (7) and (8), the span-wise circulation was calculated, and the results are shown in *Figure 19* over the desired range of angles of attack.

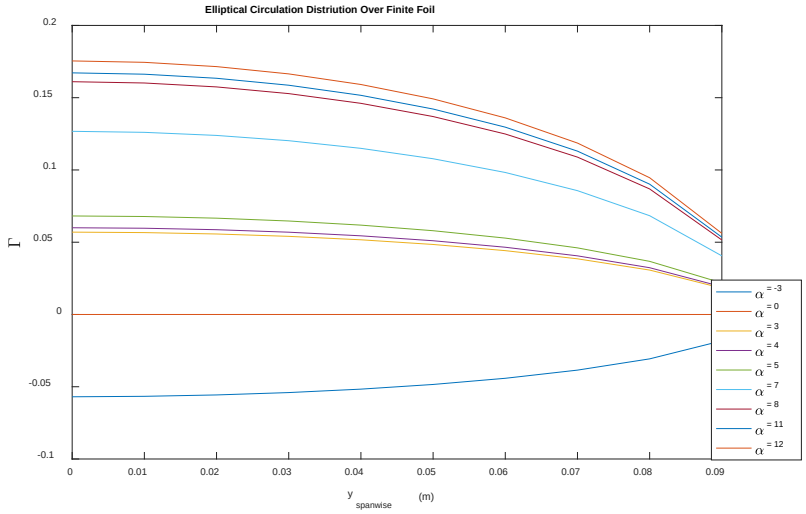

Figure 19: Span-Wise Circulation Across Wing

Since the calculation of span-wise circulation does not consider aspect ratio, the circulation is most likely larger over the End Cap foil due to the small aspect ratio. The results of the downwash and effective angle of attack calculations are shown in *Table 2*.

Table 2: Downwash and Effective Angle of Attack as Described in Figure 19

α (deg)	w (m/s)	α_{eff} (deg)
-3	0.2997	-2.94
0	0	0
3	-0.30	2.94
4	-0.32	3.94
5	-0.36	4.93
7	-0.67	6.87
8	-0.85	7.83
11	-0.88	10.82
12	-0.92	11.81

The results of the lift and drag coefficient calculations from the 3-D and 2-D calculations (12) – (14). The resulting 3-D coefficients are compared to the 2-D and experimental data in *Figure 20.*

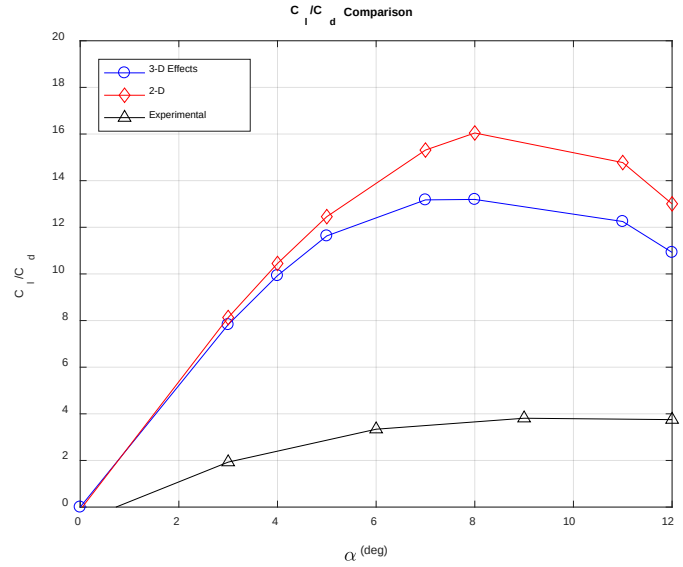

Figure 20: Comparison of 2-D, 3-D and Experimental Lift and Drag Coefficient Ratios

Figure 20 shows that the analytical solution does not match well with the experimental data. To further investigate the cause of this discrepancy, *Figure 21* and

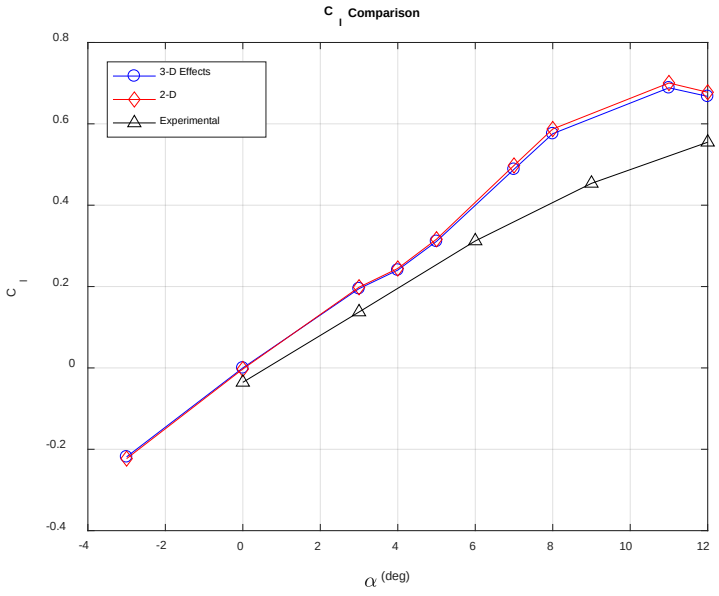

Figure 21: Comparing Lift Coefficients

Figure 22 show the separate lift and drag coefficient comparisons.

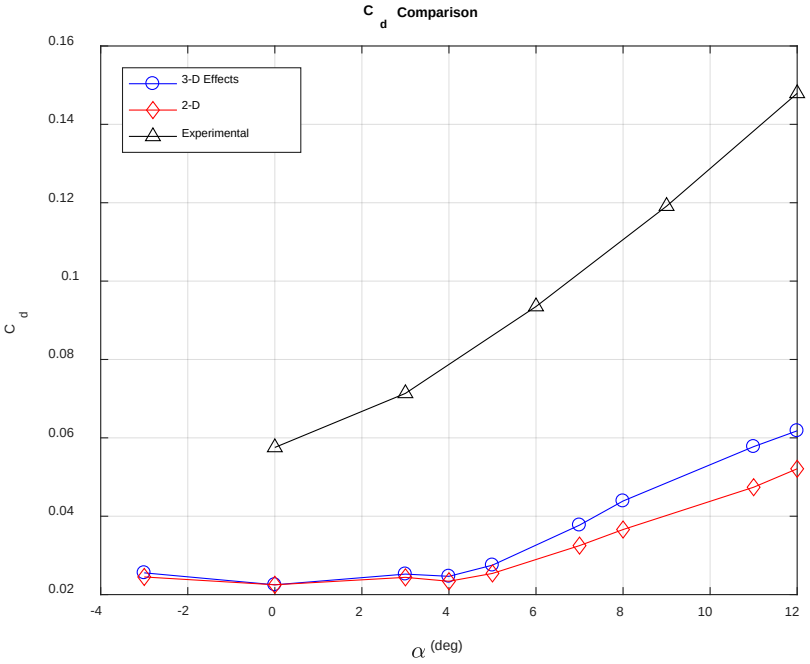

Figure 22: Drag Coefficient Comparison

Analyzing the lift and drag coefficient separately yields a clear reason for the deviations between the analytical and experimental C_L/C_D ratios. It can be seen that the lift coefficients from the analytical model are close to the experimental values, and are not the source of the large error. The small difference between the experimental and analytical lift coefficient results is most likely due to the actual induced angle of attack being slightly higher than the calculated. From the analysis of the drag coefficients, it is clear that the drag was the main source of the error between the analytical and experimental analysis. The XFOIL code uses potential flow theory, which does not solve directly for drag. It uses an approximation that tends to underestimate the drag coefficient in the 2-D realm. In addition, the finite wing corrections significantly undercompensate for the 3-D effects because of the small aspect ratio of the wing in question. Analyzing the correction factors used, it is seen that these factors were designed for larger aspect ratio foils, where much of the wing operates essentially 2-D. A final source of error is that some source of drag may have been overlooked during the analytical analysis.

6.2 Lift and Drag Analysis: End Cap vs General

When comparing foil and wingtip devices for marine and aerospace applications, it is always desirable for a device to have higher lift and lower drag, except for a few rare occasions. To allow for a true comparison of device performance, the lift and drag coefficients are used to allow for a dimensionless comparison. Since the performance of a lifting device (foil or wingtip for the applications described here) is a measure of the lift and the drag, it is ideal to find a relation that allows for the comparison of the two to allow for easy overall viewing of efficiency. To do this, the C_L/C_D ratio profile is created over a range of angles of attack. For the analysis of the

End Cap and General wingtip devices, both yielded statistically consistent results for flow speeds of approximately 9 m/s in the HiCaT. This flow speed in the HiCaT corresponds to a Reynold's number of ~670x10^3. Angles of attack of 0°-12° were analyzed, as previous studies had found that the peak performance of each wingtip device occurred over this range. *Figure 23* shows the results of the performance curve analysis. It was seen that at all angles of attack the General wingtip had a higher lift-to-drag ratio (lift-loss efficiency).

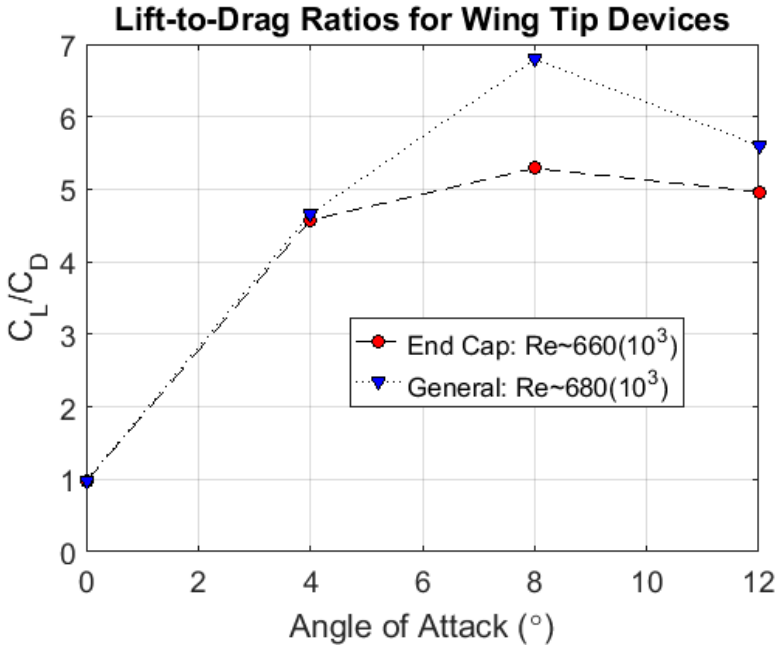

Figure 23: Performance results of the different wingtips.

6.3 Overview of Cavitation Profiles

When analyzing cavitation, it is desirable to look at how different flow and system characteristics effect the inception of cavitation. To allow for this analysis to be compared to other experiments with different experimental setups, the system and flow characteristics must be nondimensionalized. To set up a non-dimensional analysis, the cavitation number at cavitation inception is plotted against the coefficient of lift, coefficient of drag, Reynold's number, and angle of attack. Though the angle of attack is not a non-dimensional variable, it can give valuable insight into if and how the cavitation number at inception changes across the desirable range of angles of attack. This desirable range can be characterized as one that includes the peak value of the C_L/C_D ratio. With the prior knowledge from lift-drag characteristic testing of the wingtips, and from previous studies, the angles of attack range of 0°-12° was used for this cavitation inception study.

Figures 25 and *26* on the following page show all inception data points gathered during experimentation for the Endcap and General wingtips. This data includes "possible" and "definite" cavitation inceptions. From the plots of cavitation number vs Reynold's number, it can be seen that there seems to be a power trend apparent in both. It is also apparent that there appears to be a slight linear increasing trend with

an increase in angle of attack. This could possibly describe and show why the slope value, K, increases with angle of attack. This should be expected, as inception should occur at higher flow pressures since at higher angles of attack there is a greater pressure difference leading to the backside of the wingtip having a much lower pressure. The data also shows a somewhat linear trend spaced out by angle of attack within the coefficient of lift plot. As for the coefficient of drag relation, not much can be concluded from it. There can be seen a slight linear trend for each angle of attack in the drag relation for the General wingtip.

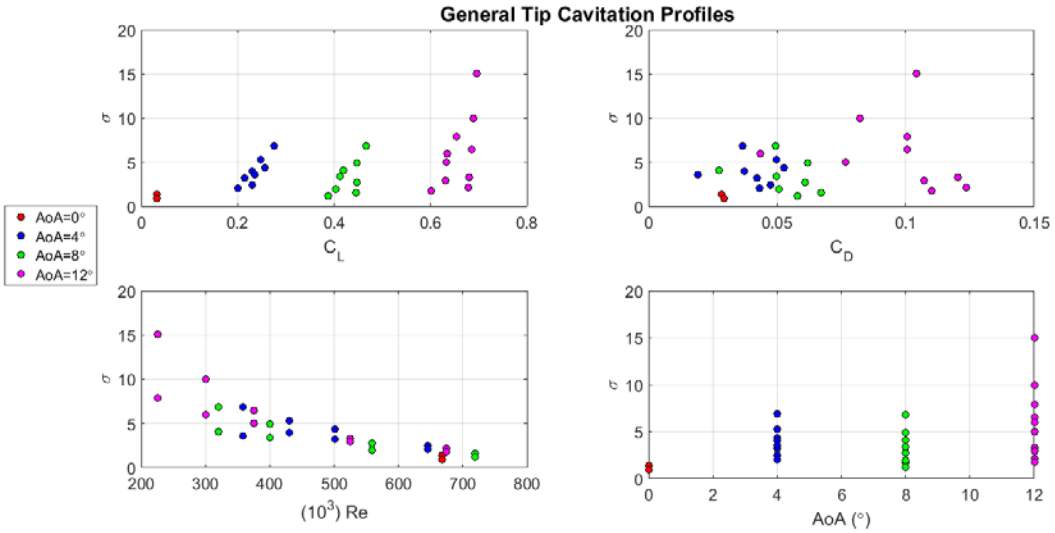

Figure 24: Cavitation data for the general tip.

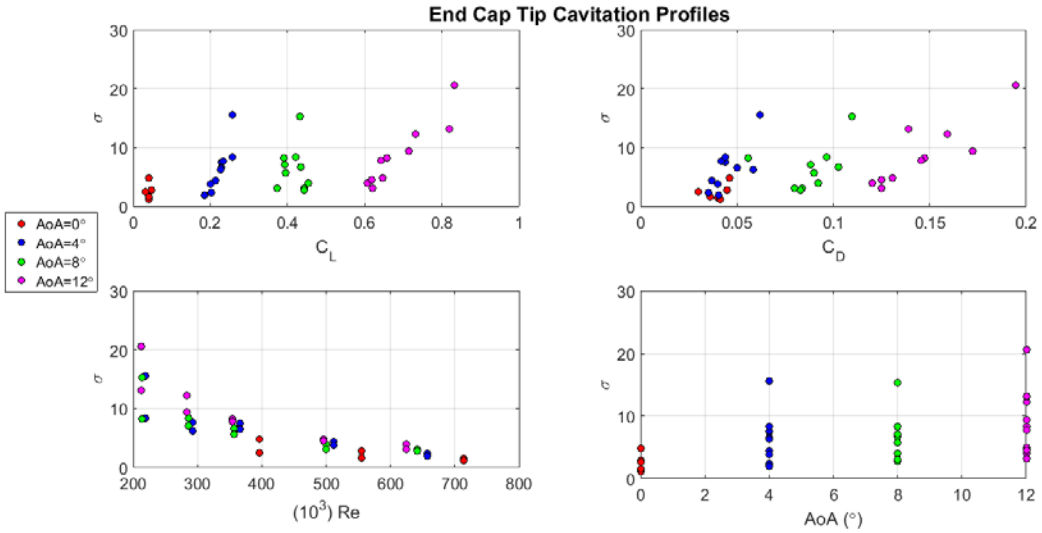

Figure 25: Cavitation data for the end cap tip.

6.4 Cavitation Inception – Analytical vs Experimental

From the analysis of the different experimental conditions for testing, it was found that the most consistent results, and most statistically relevant were gathered from the "definite" inception at high operational Reynold's numbers (RPM speeds of 700 and 900). Different analysis and data separation methods that were analyzed can be seen in the *Appendix. Figure 26* illustrates the results of the high Reynold's number test data applied to (5). From what is expected from previous studies, the End Cap data should fall nicely within and around the minimum and maximum K slope lines. As for the expected results for the General wingtip, the data should fall below, and is expected to possibly follow a different trend than that found in previous studies for elliptically loaded foils.

From the analysis of Figure *26* it can be seen that the first data clustering, which corresponds to an angle of attack of 0°, falls well above the expected linear trends. This error is easily explained as cavitation at low angles of attack occurs much earlier on the foil itself than on the tip. This early cavitation on the foil leads to an induced cavitation on the tip of the wing, but this is not the actual cavitation point that is desired based on descriptions from previous studies. The other data for the End Cap falls within the acceptable range, and thus can be seen to follow the expected trends. The data for the General foil is seen to be below that of the End Cap as expected, and this means that the addition of the General tip mitigates cavitation at some level. It is seen that the General data falls at lower slope values which is what has been seen in previous studies. The values themselves, fall below that of previous results for the General wingtip.

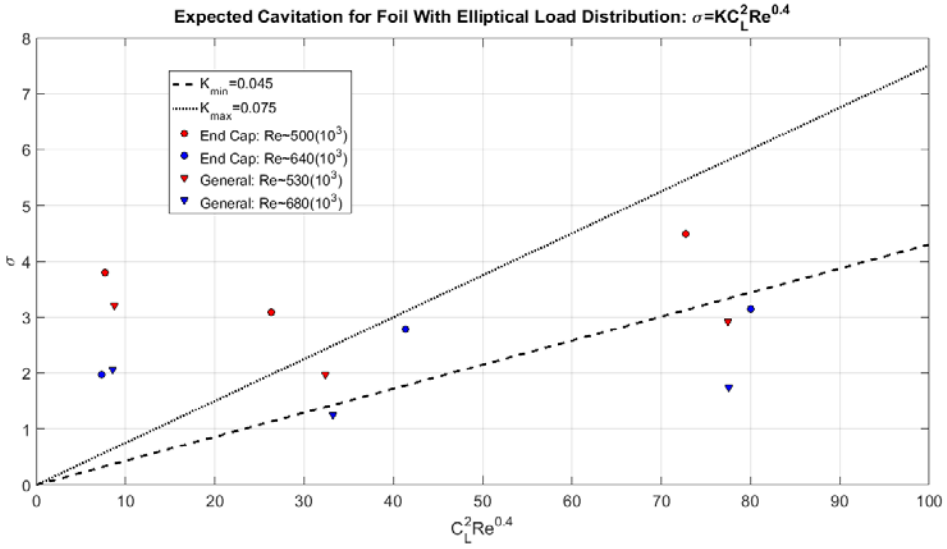

Figure 26: Comparison of analytical and experimental inception of cavitation.

6.5 General Tip – Fitting of Data

Since it is known that the inception profile for a non-elliptically loaded hydrofoil should deviate from that of an elliptically loaded hydrofoil, and as shown in Section 6.4 the data agrees, it was desirable to look into a possible universal relation to

describe inception for the General wingtip. From the analysis of previous studies, it was found that depending on angle of attack the slope coefficient, K, changed. Since this leads to several relations for inception depending on a devices geometric orientation, it was seen as desirable to unify the data set under one relation taking the change in slope into account. This was done performing an optimization analysis for the coefficient of correlation for a linear fit through the data that originated at the point (0,0). To allow for the compensation of a changing K value over angles of attack, (15) was used, and values of 'a' and 'b' were varied over the range of -5 to 5 at an interval of 0.01 to find the "ideal" formulation.

$$\sigma = KC_L^a Re^b \tag{15}$$

The large range of values for 'a' and 'b' were used to allow for any strange deviations to be captured, and all basis to be covered in terms of getting the "ideal" relation.

Figure 27 shows the results of this optimization. The final formulation of (15) was found to be:

$$\sigma = 8965(10^9)C_L^{-0.05}Re^{-2.1} \tag{16}$$

This relation was found to have the optimized correlation of coefficient which was found to be $r^2 = 0.8729$, meaning that 87.29% of the data variations are explained by the linear regression. This formulation is far from what the relation was found to be for the elliptically loaded foil, but it is believed that this deviation is caused by the inclusion of the K deviations for different angles of attack.

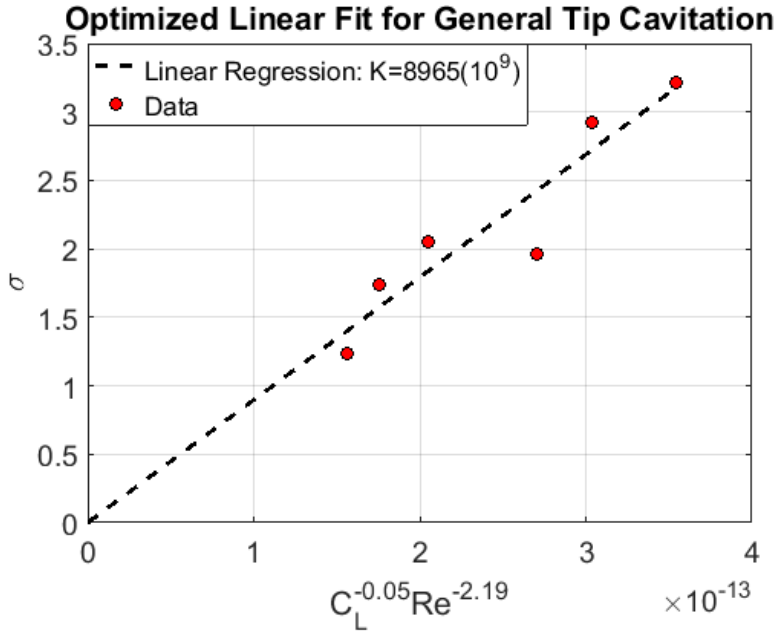

Figure 27: Optimization of experimental cavitation data.

7 Conclusions

These experiments provided valuable insight into the effect of wingtip devices on cavitation. The addition of a wingtip device does delay the onset of cavitation, causing it to occur at lower pressures. This is valuable knowledge because it could lead to increases in the efficiency of devices as well as extending their lifespans. Along with decreasing the effect of cavitation, wingtip devices improve the overall performance of a foil. The C_L/C_D ratio for a foil with a wingtip device was consistently higher than that of a normal wingtip. However, to provide more concrete results the definition of cavitation must be more objectively defined. This is the reason for the discrepancies between the experimental results and the results obtained in previous years. The definition of cavitation used by previous teams was not known and therefore could be vastly different from the definition used in these experiments. By providing a better definition for what cavitation is will allow future experiments to be carried out with greater accuracy and will provide opportunities to accurately study other wingtip devices. This, in turn, will provide valuable data for researchers and designers alike by giving them information to engineer more robust and efficient designs.

Future Development

- Design a more objective test criterion for cavitation inception and dissonance
- Understand why the sensitivity of the drag balance changes with sampling rate and number of samples collected and try to mitigate this.
- Design new mounting collar for the drag shaft so the tightening process does not interfere with force balance calibration
- Noise Reduction
    - Replace AC power supply for pressure valves with DC power supply or newer AC power supply to remove 60Hz noise in signal
    - Coil, rigidly mount, and shield force balance wires to reduce noise in wires from environmental disturbances
    - Ground HiCaT to remove the possibility of it being at a different electrical potential
- Seal the following leak locations
    - Window above rotor closest to elbow
    - Window on vertical pipe below reservoir tank
    - Lower connection of PVC filter piping to tunnel
    - Reservoir tank seal between silver metal plate and tunnel
    - Connection between fin box and vertical blue pipe closest to motor
    - Upper outer corner above motor
- Install a thermocouple into ¾" threaded opening of the HiCaT after the diffuser using reducer fitting and Swagelok to allow for real time temperature reading during testing.

8 References

[1] Ocean Renewable Power Conversion, 2016, "TidalGen Power System", http://www.orpc.co/orpcpowersystem_tidgenpowersystem.aspx

[2] Verdant Power, 2016, "Kinetic Hydropower System (KHPS)", http://www.verdantpower.com/kinetic-hydropower-system.html

[3] Wojtowicz, A., and Barret, T., 2016, "Design of Wingtips Devices for Marine Applications". B.S. thesis, Department of Mechanical Engineering, University of New Hampshire

[4] Ivaylo Nedyalkov, 2015, “Performance and Cavitation Characteristics of Bi-Directional Hydrofoils”, Ph.D. thesis, Department of Mechanical Engineering, University of New Hampshire.

[5] Arndt, R., 2002, “Cavitation in Vortical Flows”, Annual Review of Fluid Mechanics, 34, pp. 143-175.

[6] Anderson, J. D., 2001. "Fundamentals of Aerodynamics", 3rd ed., New York, NY: Mc-Graw Hill.

[7] Drela, M., n.d., "Fluids – Lecture 7 Notes: Elliptical Lift Distribution". Fluid Mechanics Lecture, Massachusetts Institute of Technology, Boston, MA.

9 Appendix

Tabulation of End Cap Modeling Used for Analytical Lift and Drag Analysis

Parameter	Value
Motor speed	528 rpm
Flow Speed	~ 5 m/s
Pressure in the HiCaT	~ 96 kPa
Temperature	20 °C

x/c	y/c
1	0
0.9825	0.018
0.975	0.024
0.95	0.035
0.9	0.048
0.85	0.057
0.8	0.064
0.75	0.069
0.65	0.076
0.6	0.078
0.5	0.08
0.4	0.078
0.35	0.076
0.25	0.069
0.2	0.064

0.15	0.057
0.1	0.048
0.05	0.035
0.025	0.024
0.0125	0.018
0	0
0.0125	-0.018
0.025	-0.024
0.05	-0.035
0.1	-0.048
0.15	-0.057
0.2	-0.064
0.25	-0.069
0.35	-0.076
0.4	-0.078
0.5	-0.08
0.6	-0.078
0.65	-0.076
0.75	-0.069
0.8	-0.064
0.85	-0.057
0.9	-0.048
0.95	-0.035
0.975	-0.024

0.9825	-0.018
1	0

Alpha	CL	CD
-8	-0.6371	0.03663
-7	-0.5021	0.03259
-6	-0.3635	0.03036
-5	-0.2697	0.02544
-4	-0.2371	0.02338
-3	-0.2254	0.02445
0	0	0.02254
3	0.2255	0.02443
4	0.2375	0.02338
5	0.2698	0.02541
7	0.5016	0.03253
8	0.6375	0.03658
11	0.6617	0.04737
12	0.6944	0.05214
13	0.67	0.05903
14	0.6172	0.06949
15	0.5335	0.08644

OpenFOAM

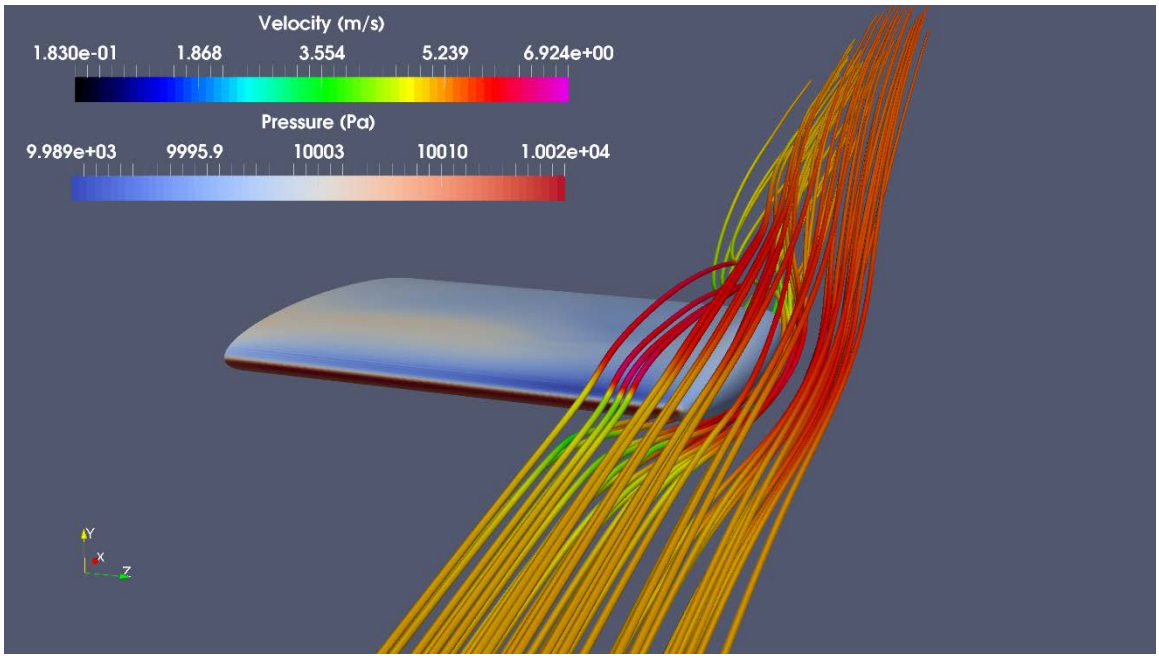
Velocity (m/s)
1.830e-01
1.868
3.554
5.239
6.924e+00
Pressure (Pa)
9.989e+03
9995.9
10003
10010
1.002e+04
Y
X
Z

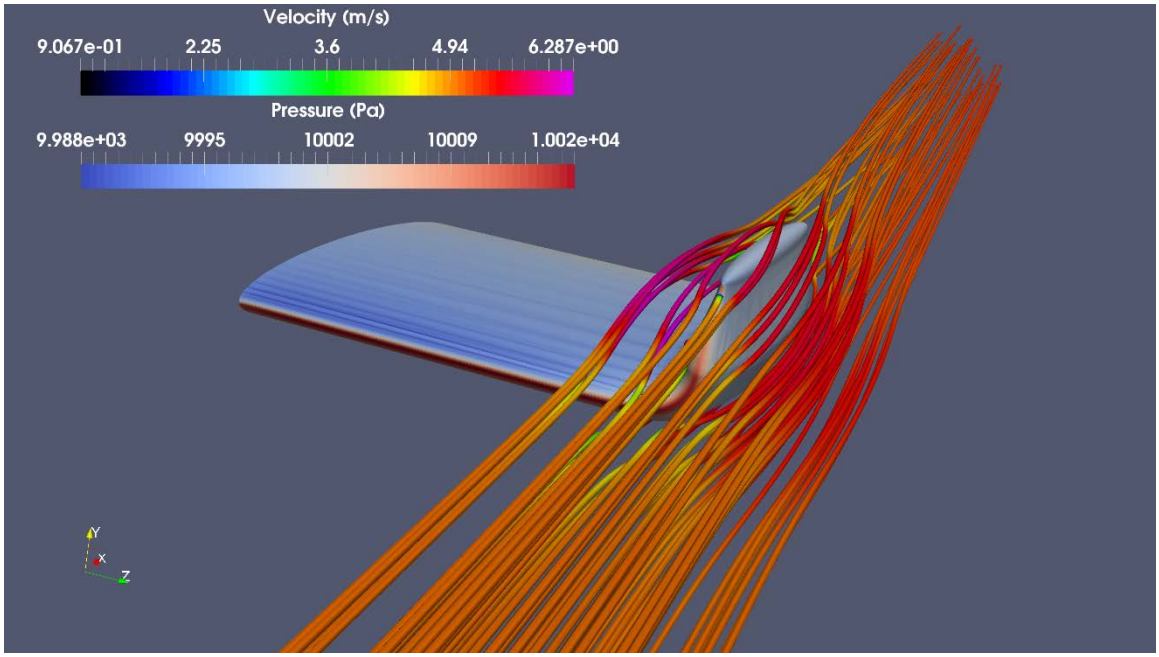
Velocity (m/s)
9.067e-01
2.25
3.6
4.94
6.287e+00
Pressure (Pa)
9.988e+03
9995
10002
10009
1.002e+04
Y
X
Z

Lift and Drag Analysis from Cavitation Results

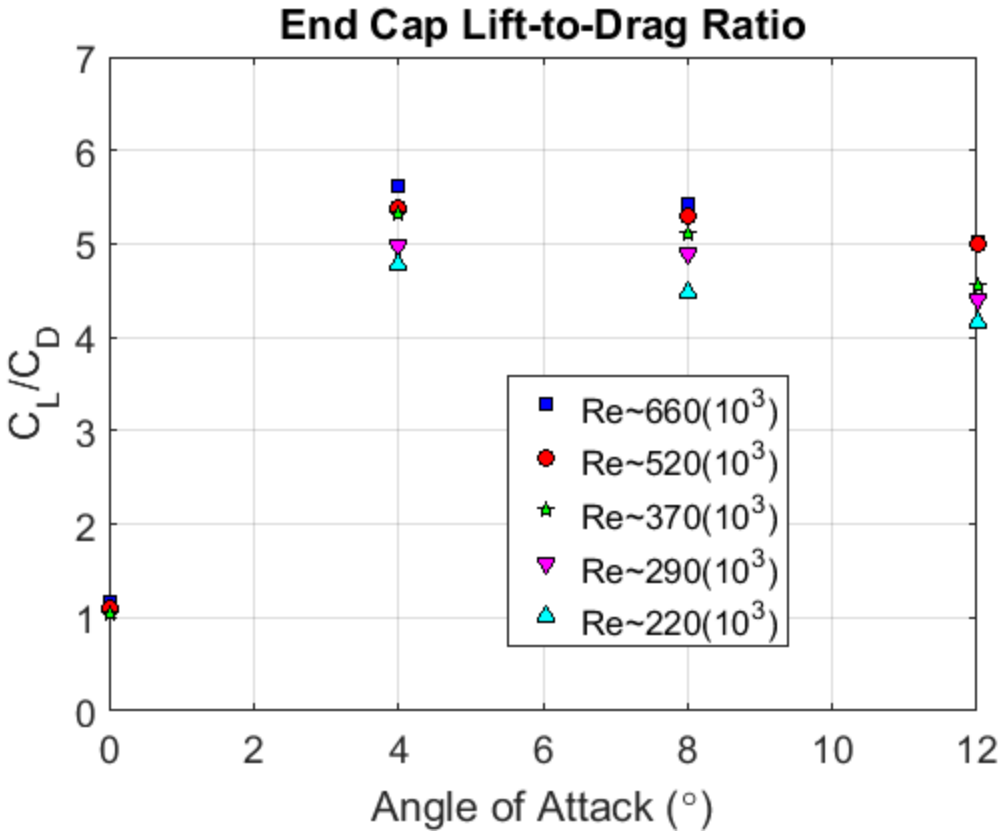

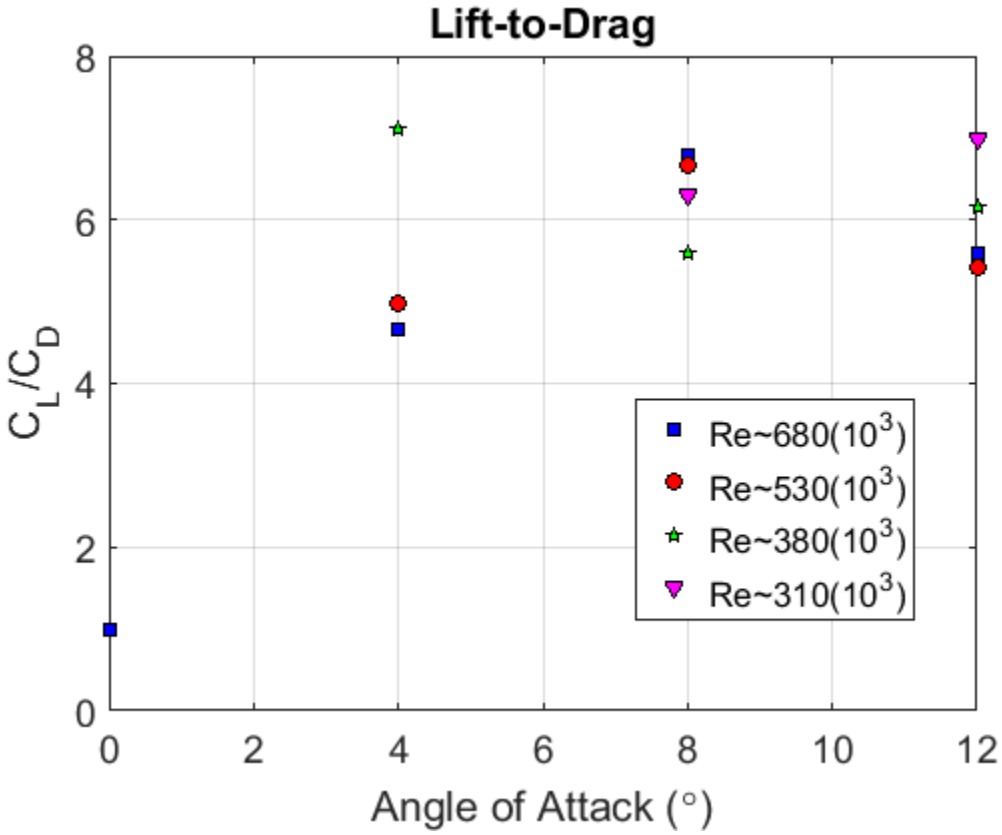

Methods of Data Analysis Results

--END CAP

All Inception

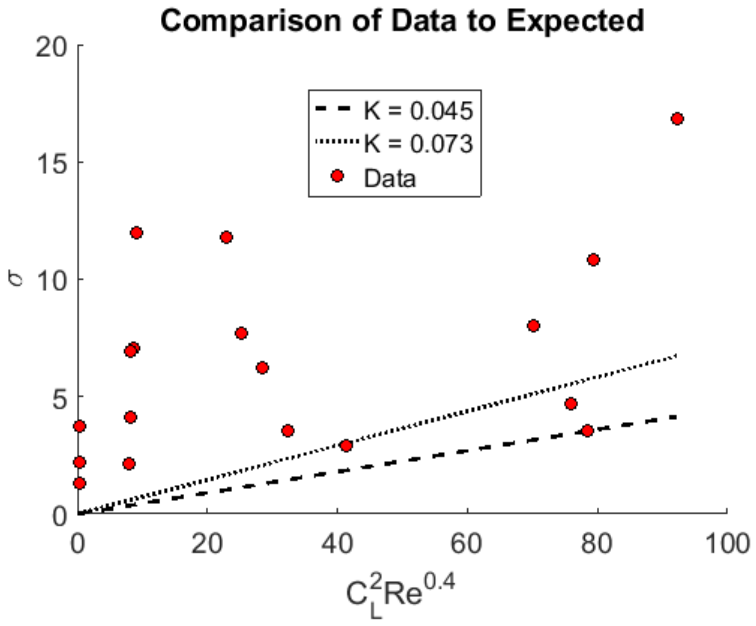

Possible Inception

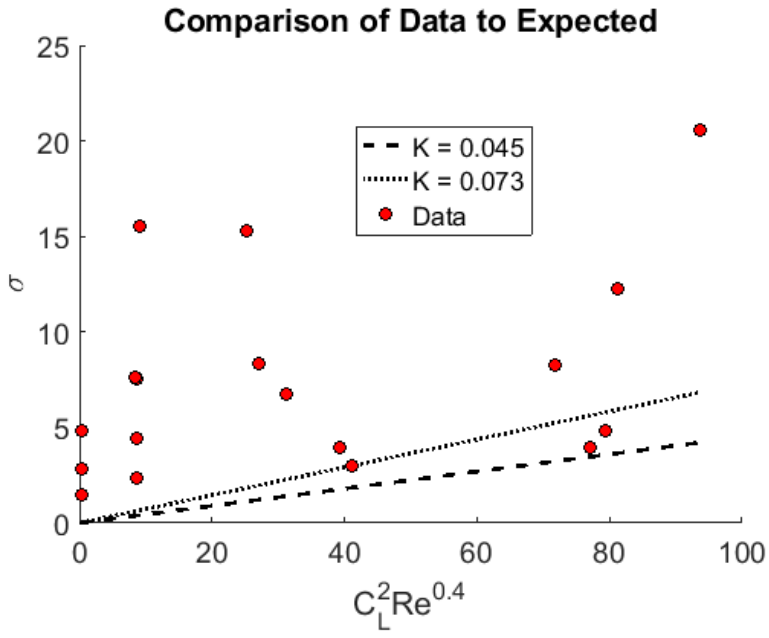

Definite Inception

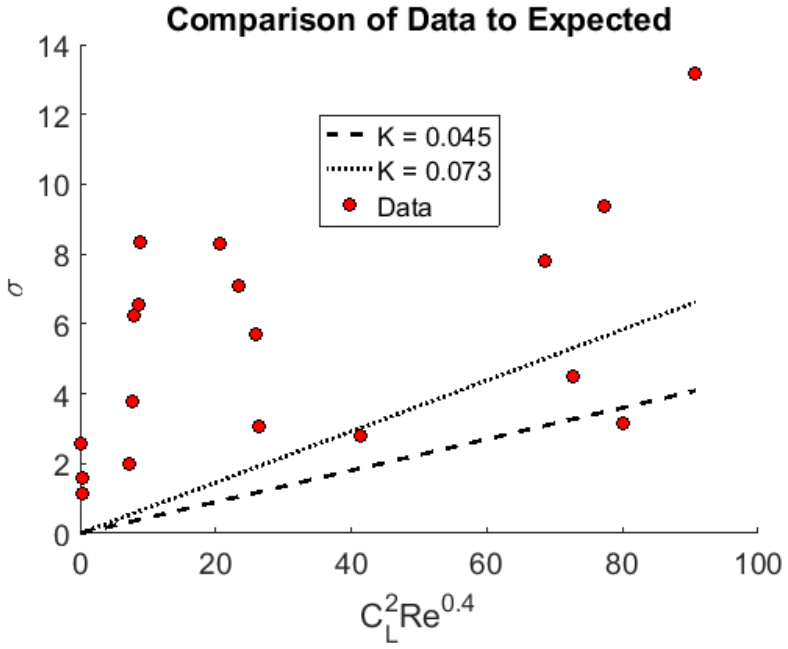

All, Low Speed

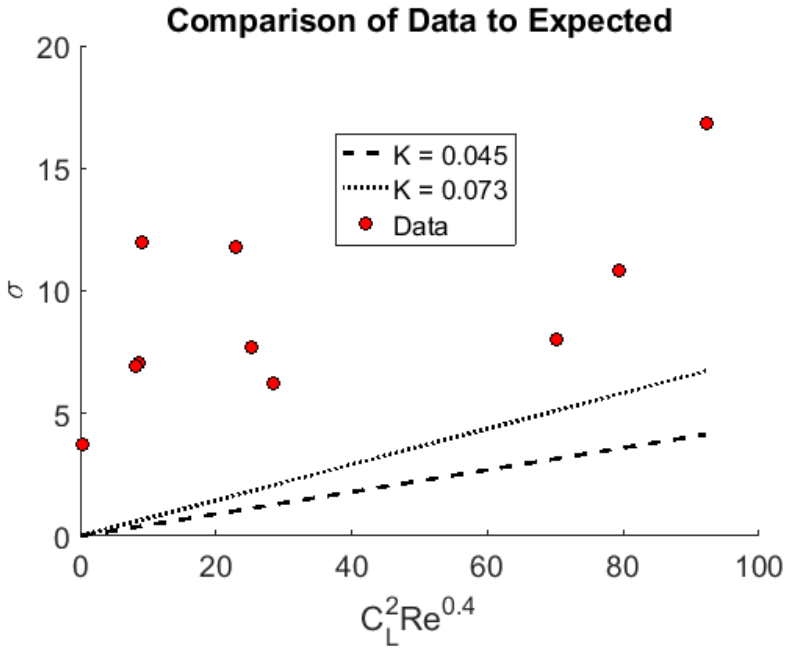

All, High Speed

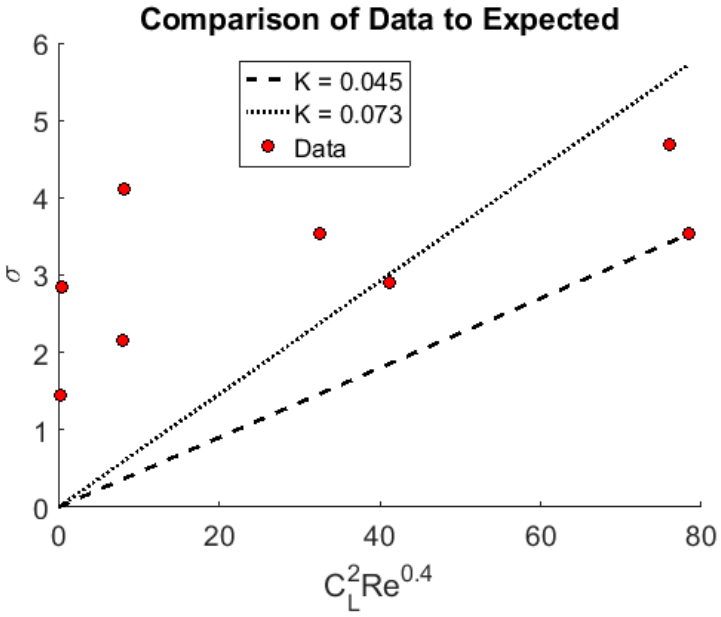

All, Low AoA

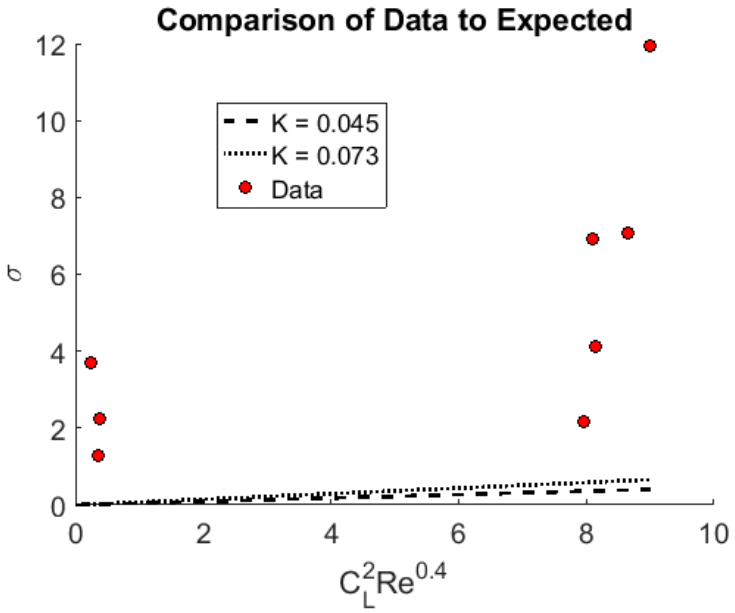

All, High AoA

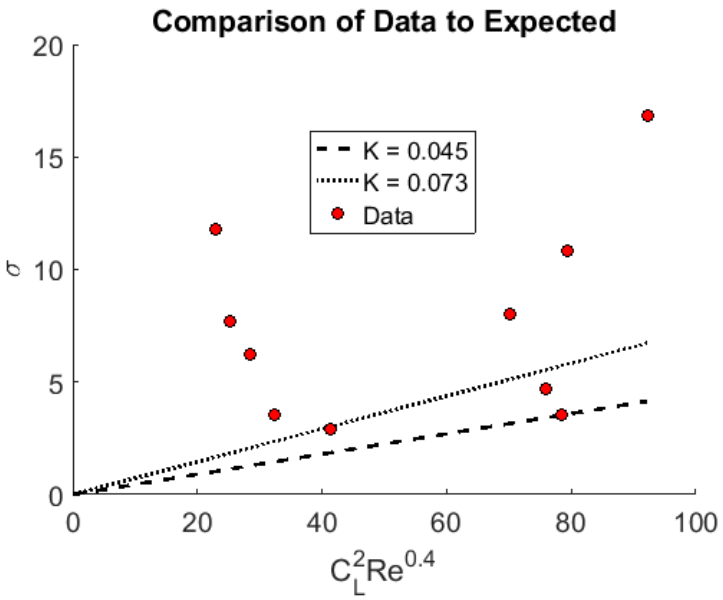

Possible, Low Speed

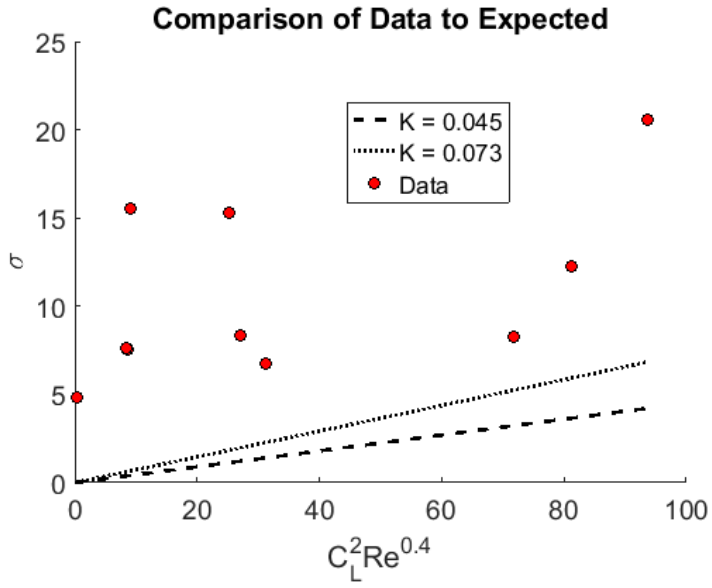

Possible, High Speed

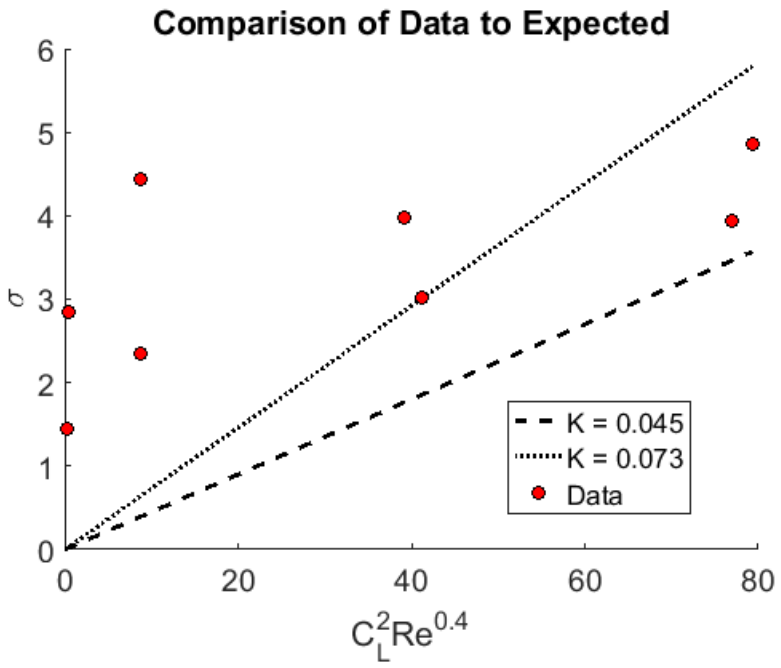

Possible, Low AoA

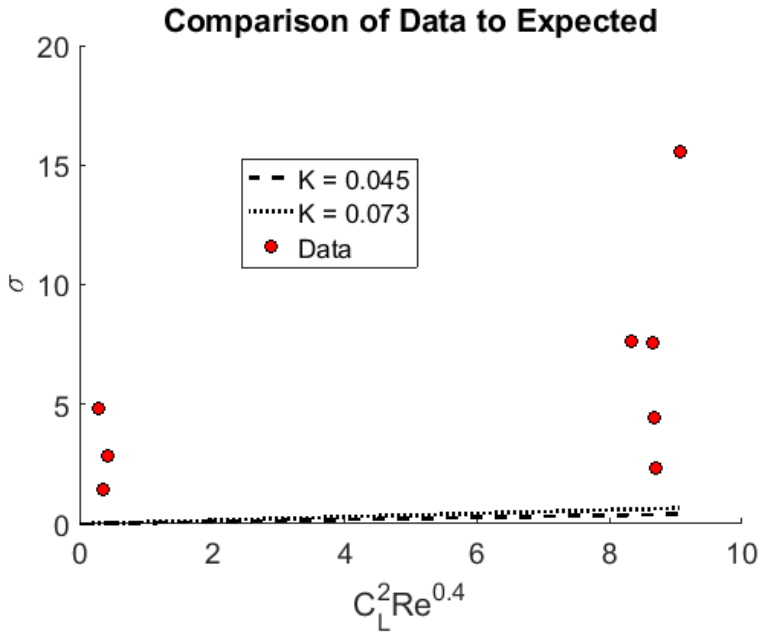

Possible High AoA

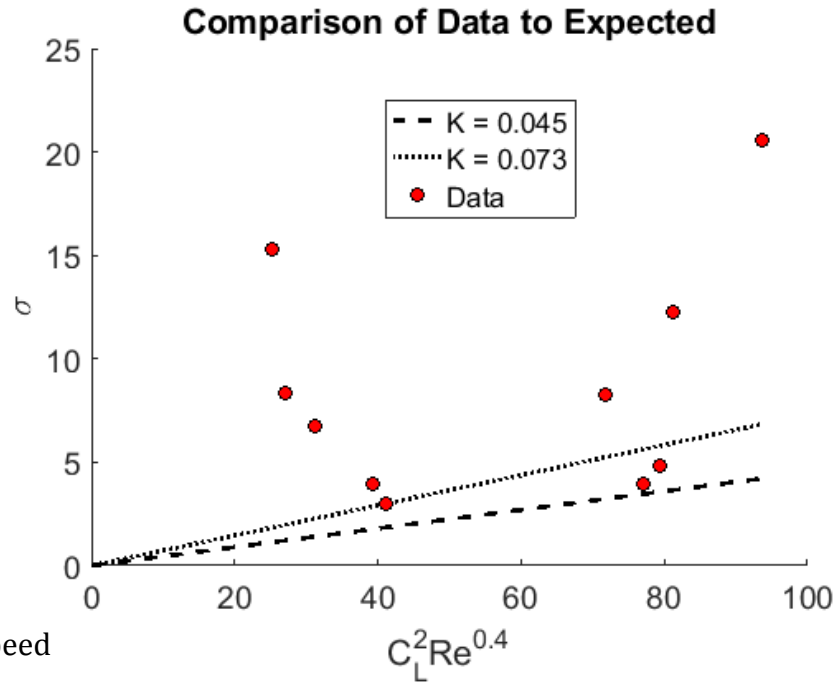

Definite, Low Speed

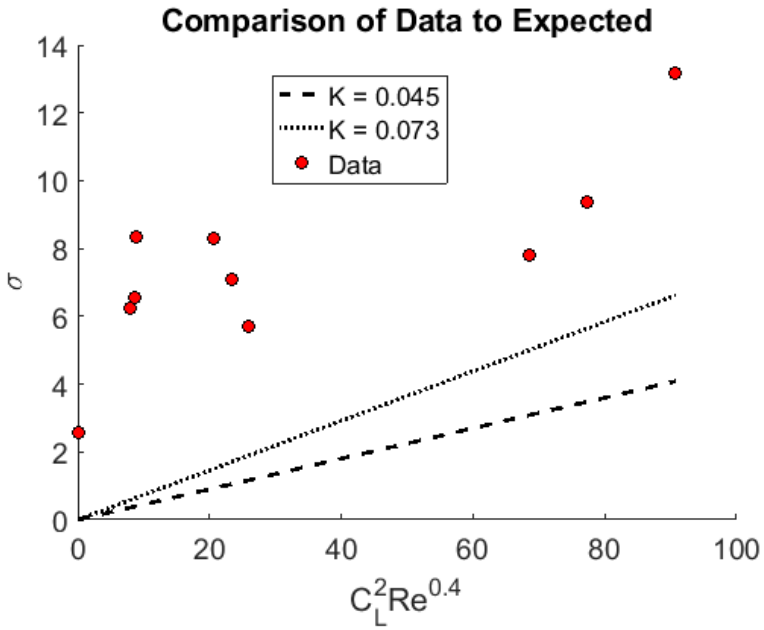

Definite, High Speed

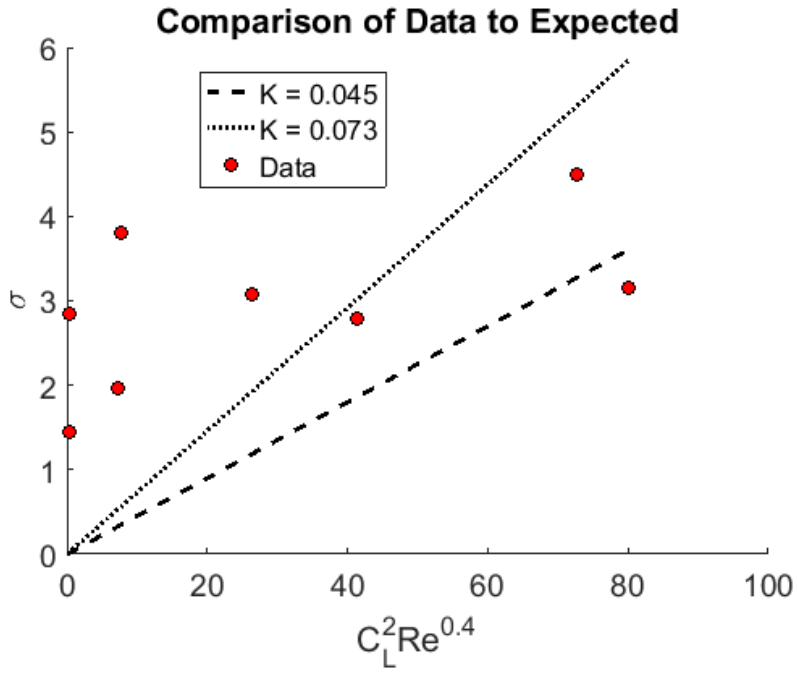

Definite Low AoA

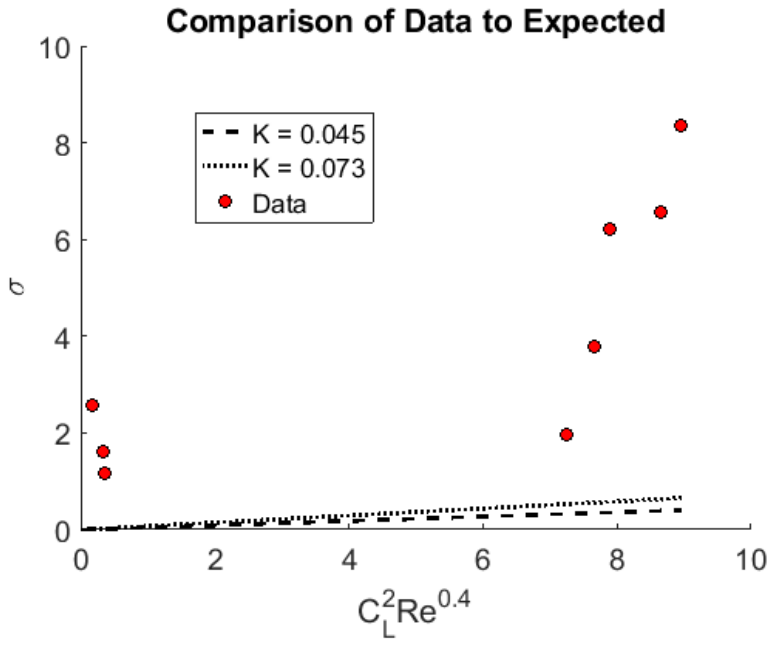

Definite High AoA

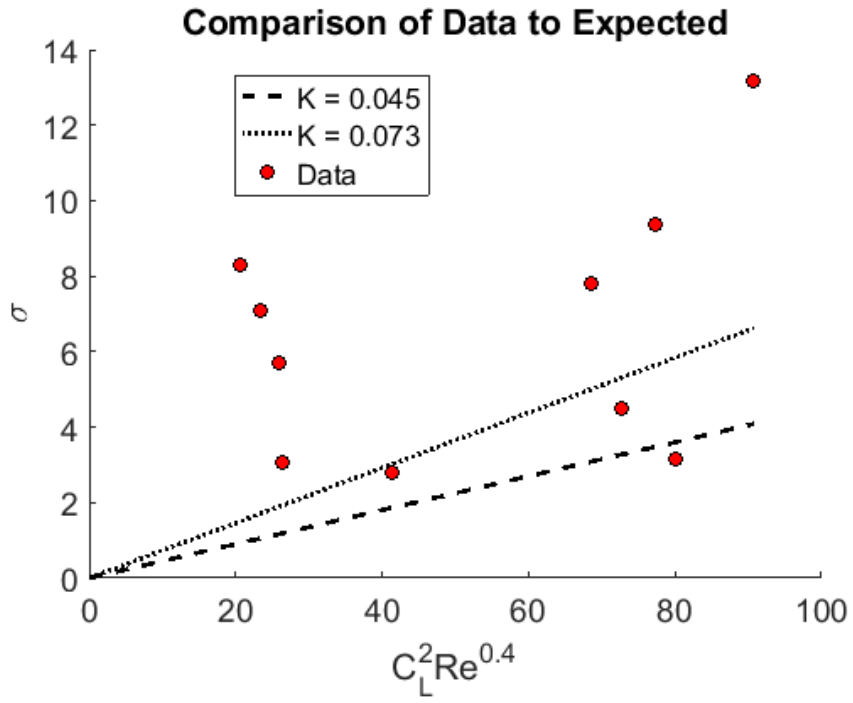

--GENERAL

All Inception

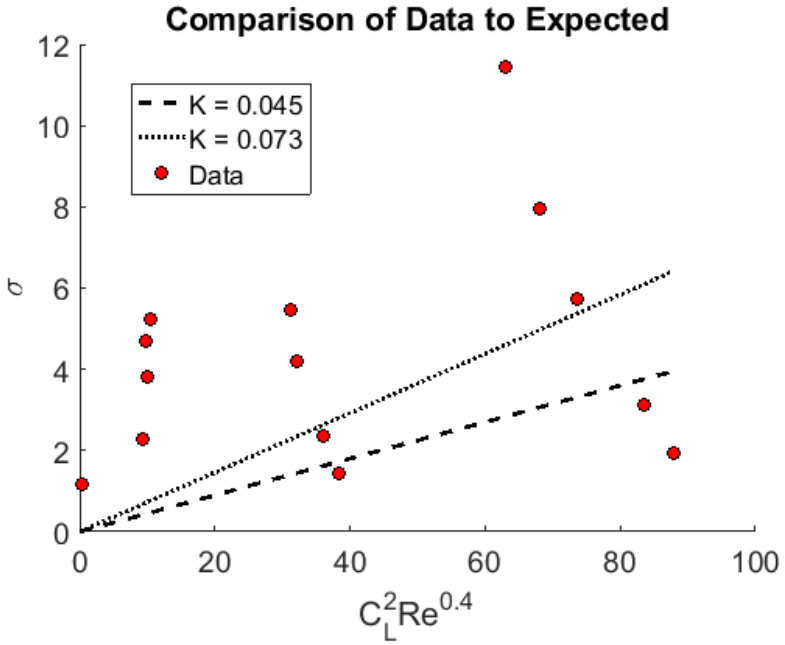

Possible Inception

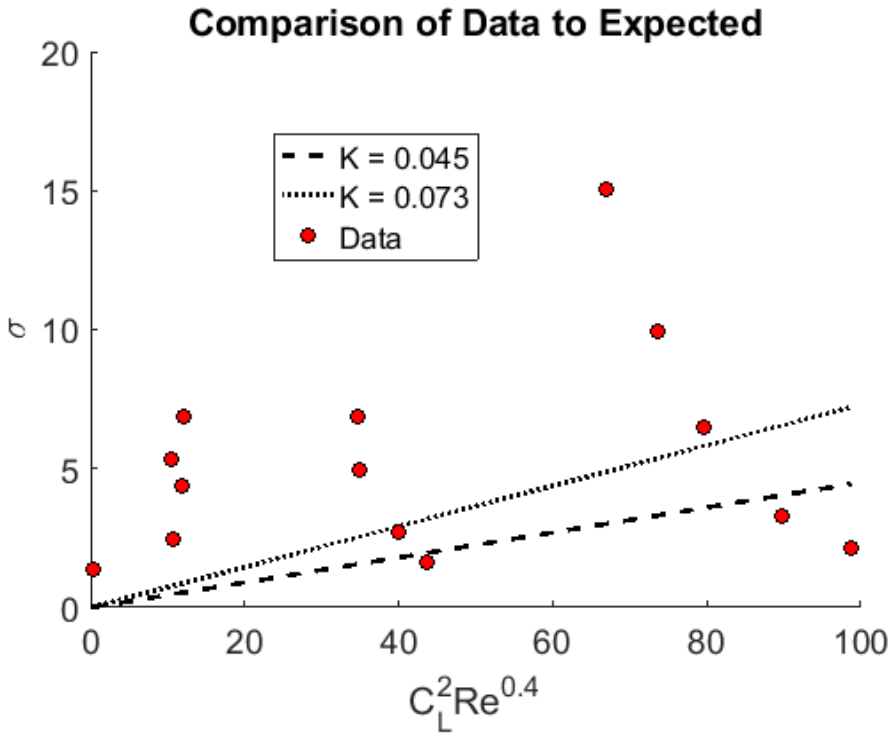

Definite Inception

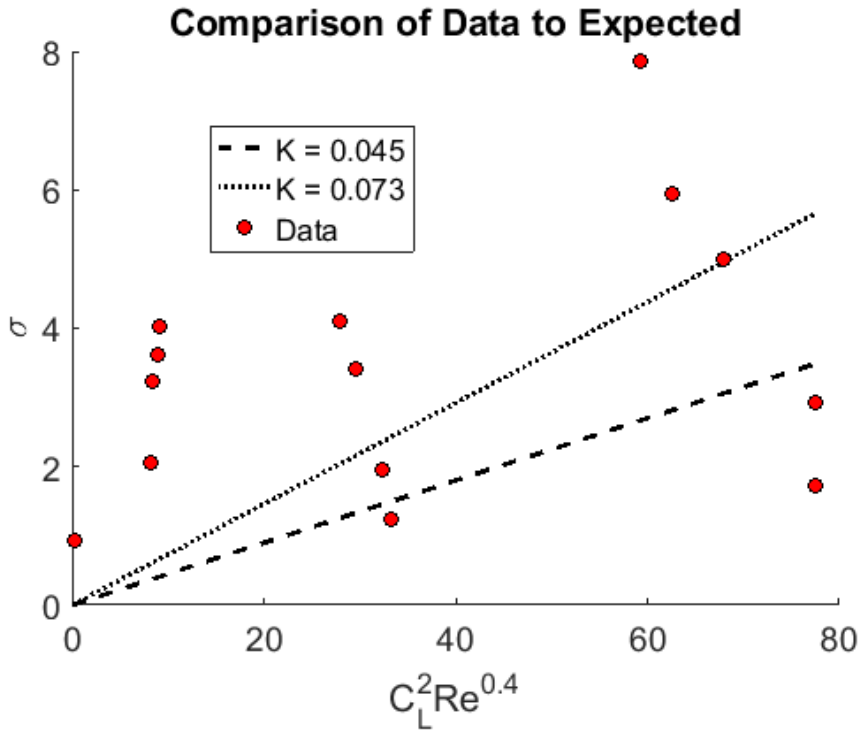

All, Low Speed

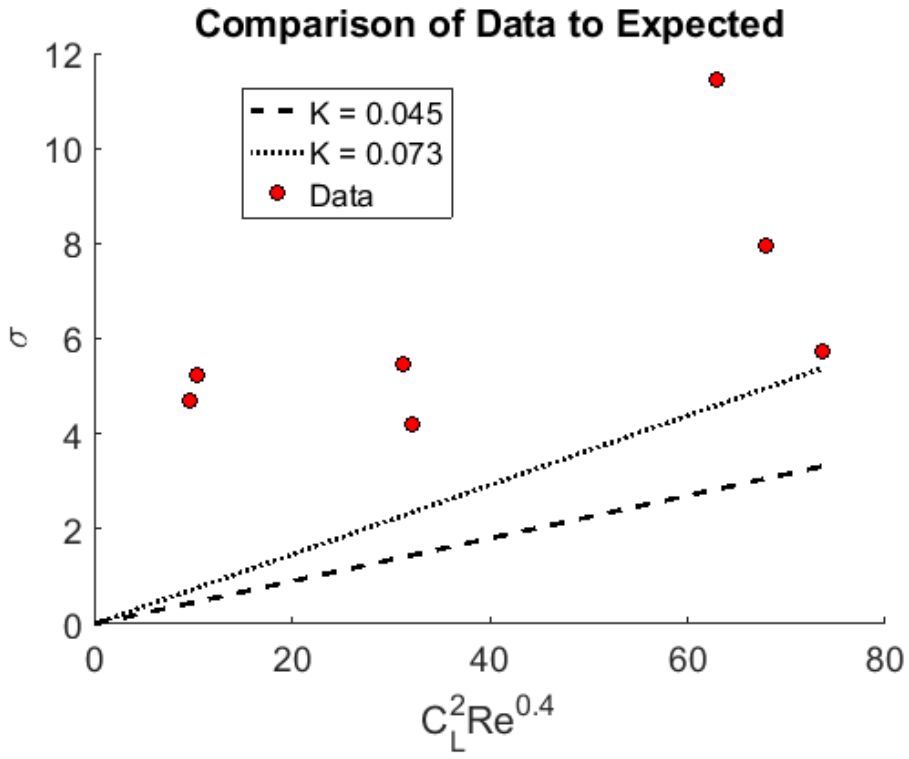

All, High Speed

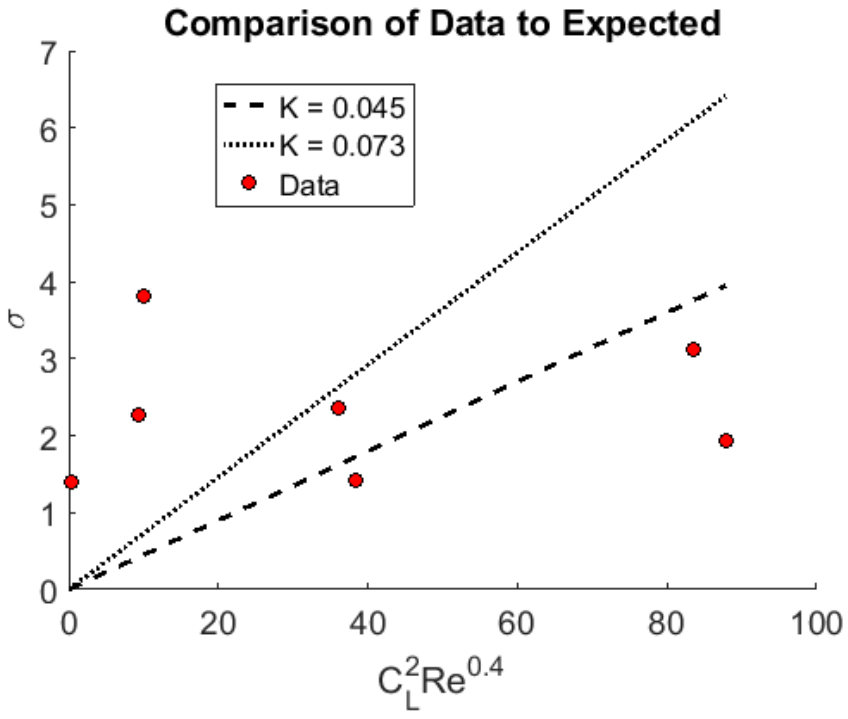

All, Low AoA

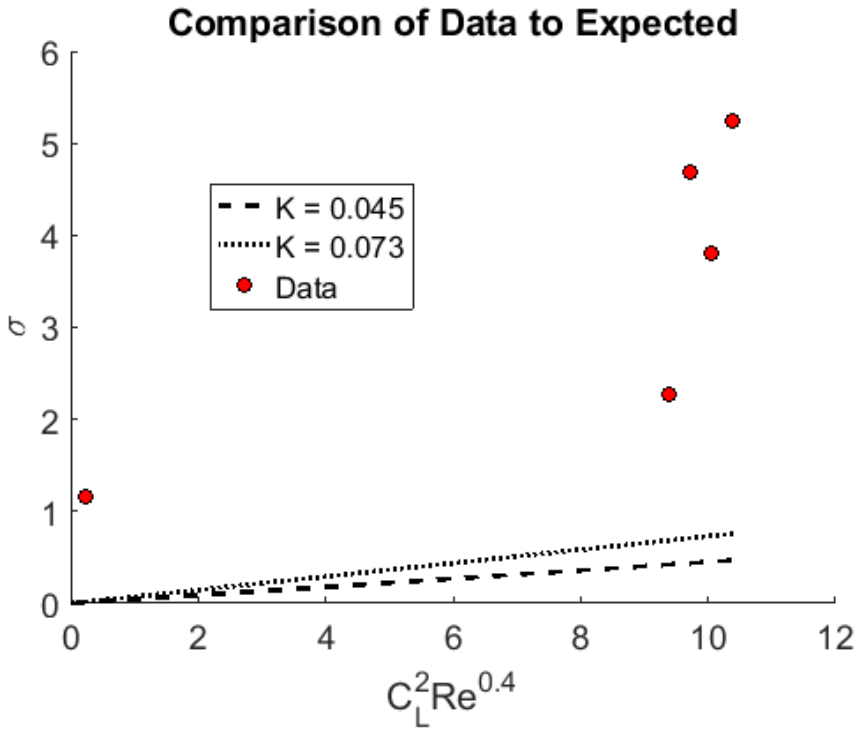

All, High AoA

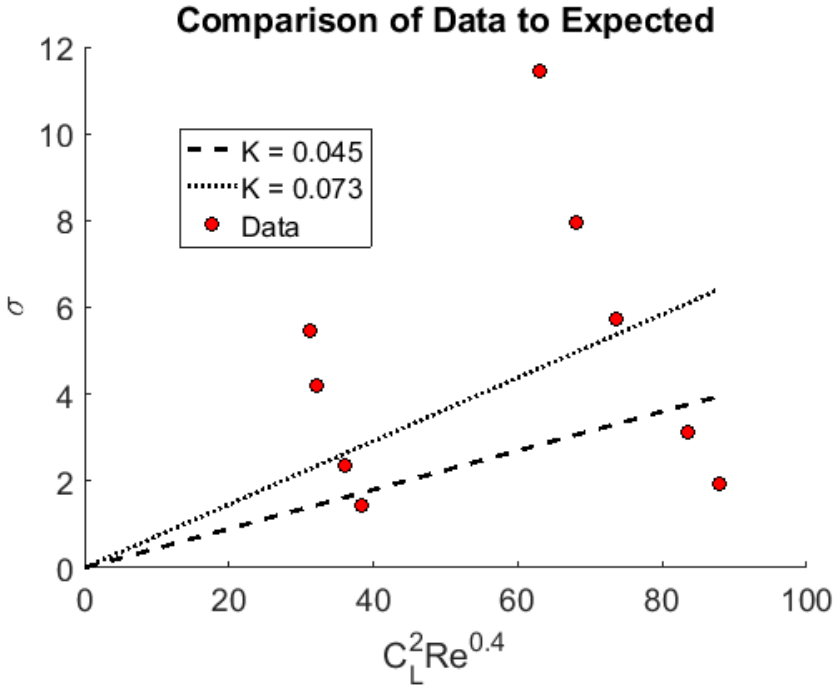

Possible, Low Speed

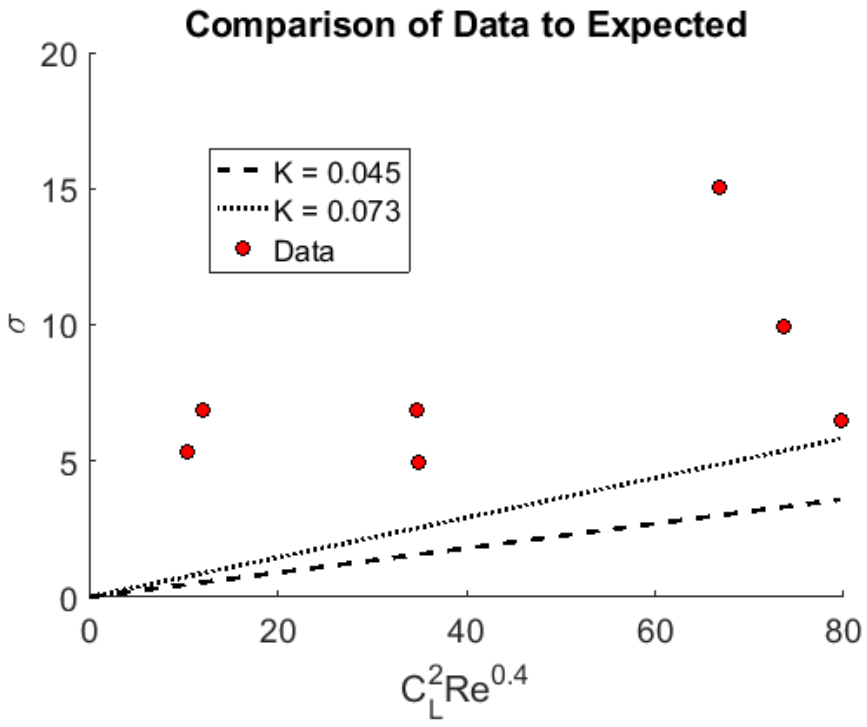

Possible, High Speed

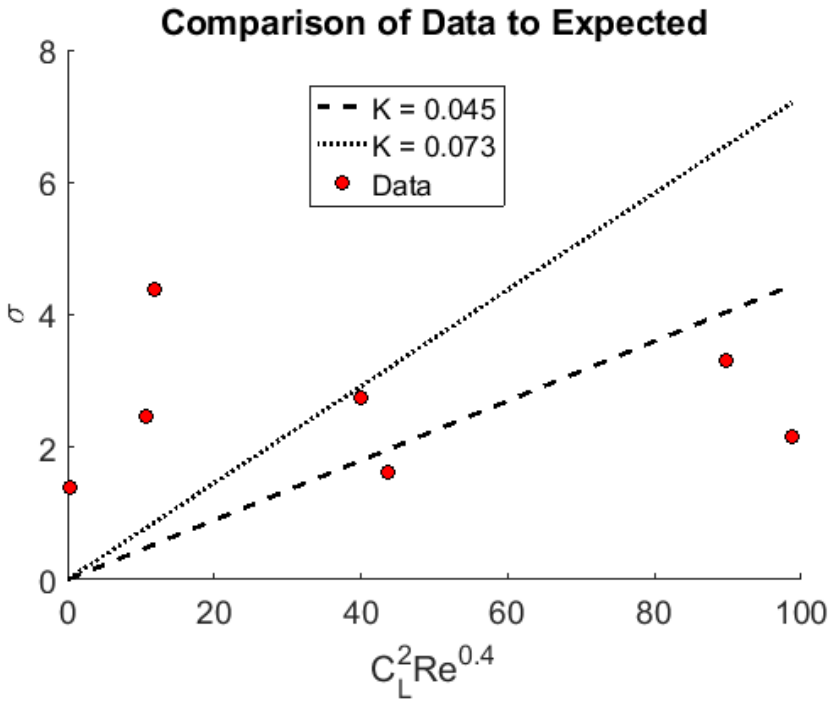

Possible, Low AoA

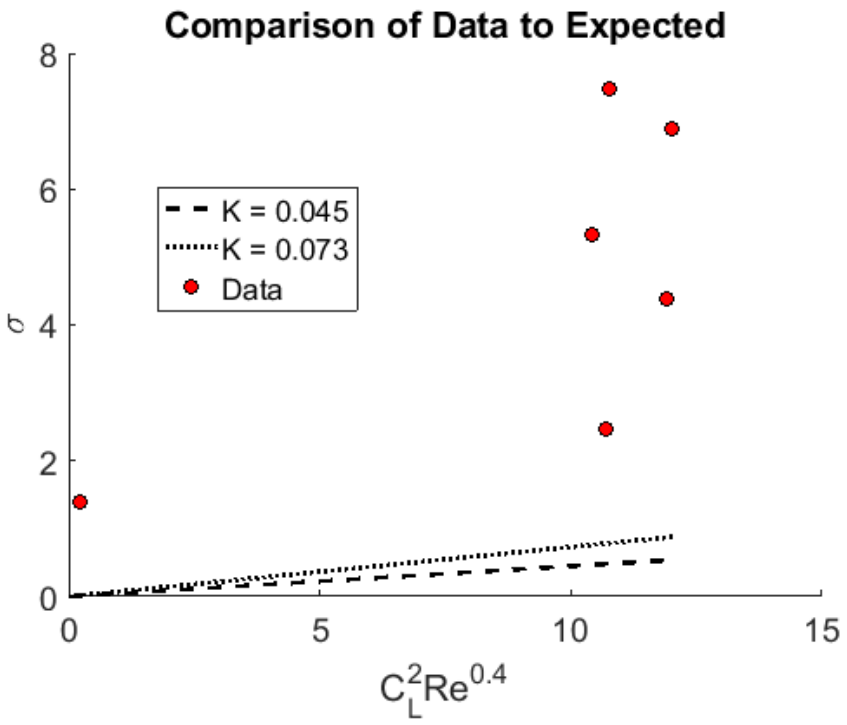

Possible High AoA

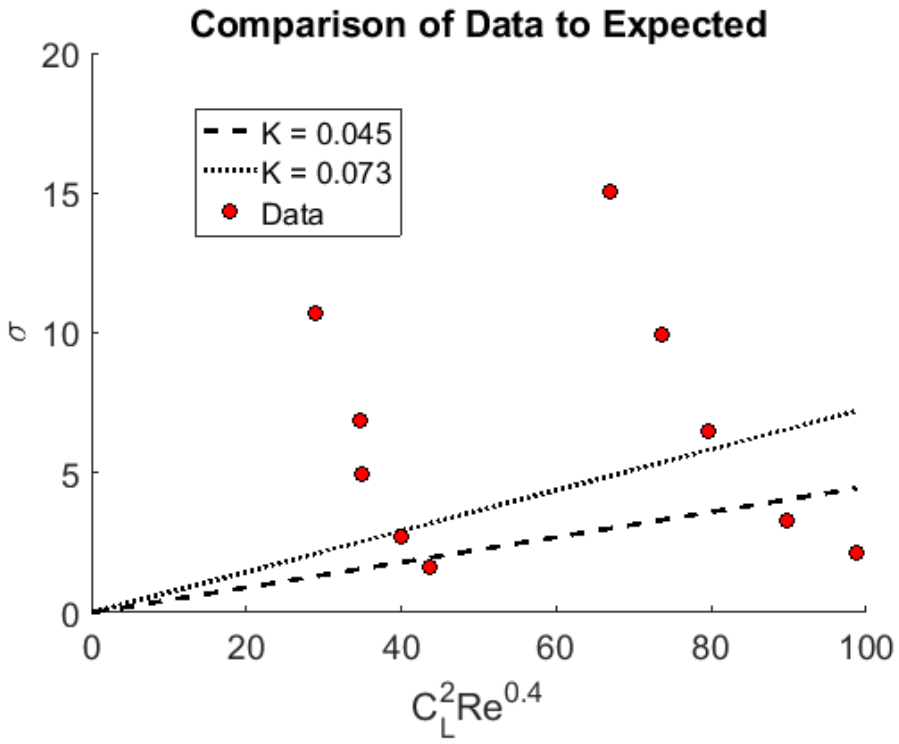

Definite, Low Speed

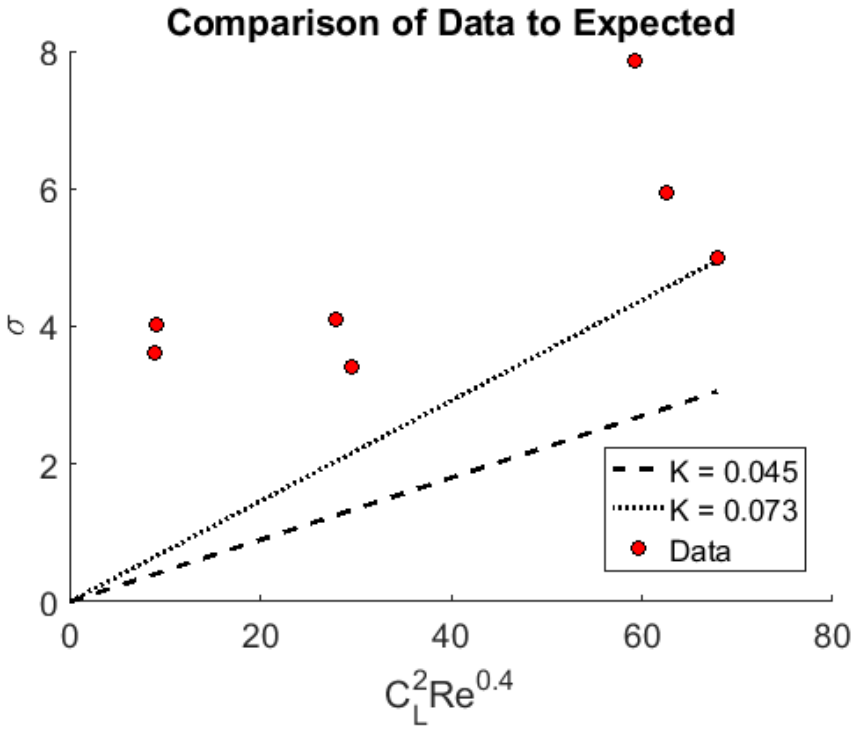

Definite, High Speed

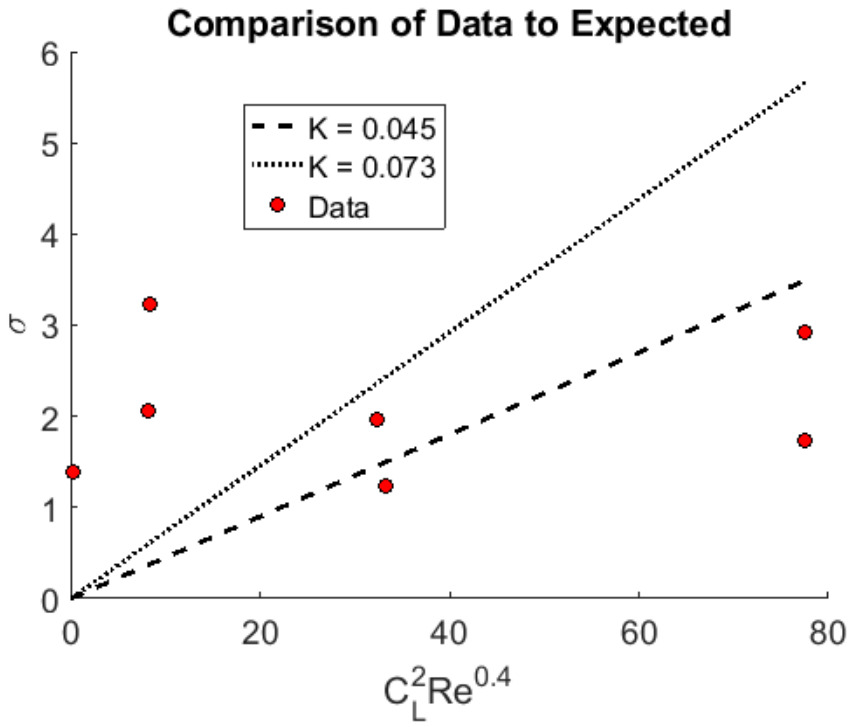

Definite Low AoA

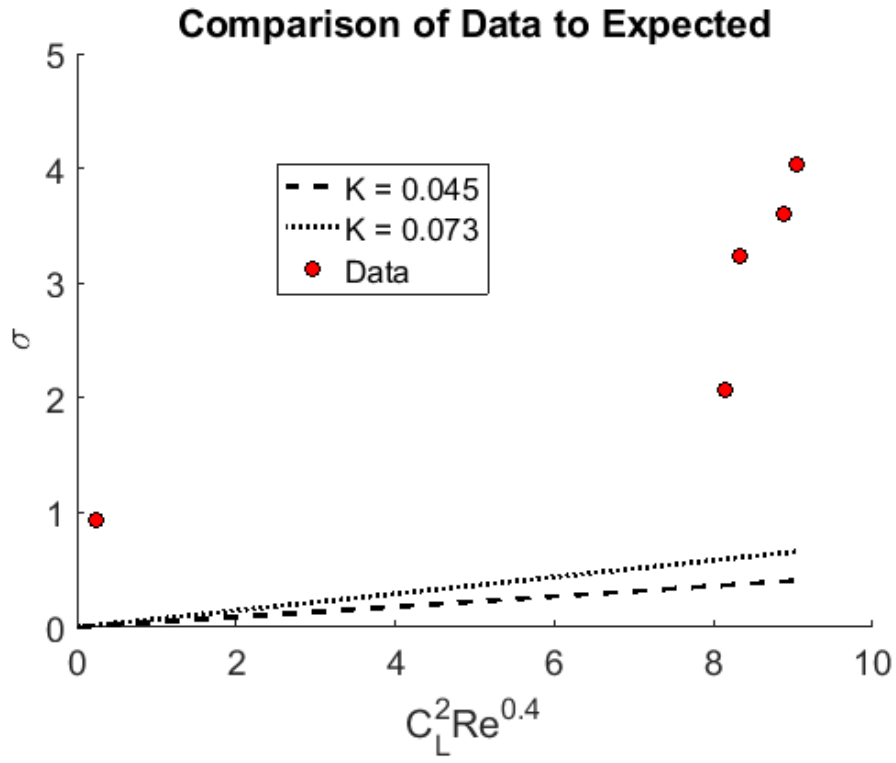

Definite High AoA

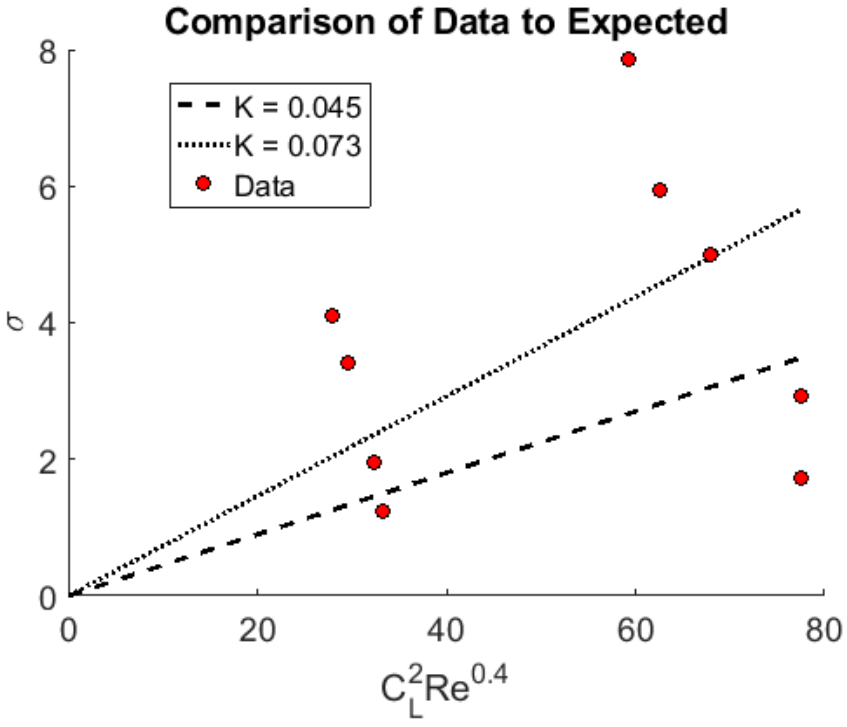

Calibration Matlab

```
function [pop_t] = Cali_Cons_Single(L_or_D,Calibration)
```

Data Input

```
data = importdata(Calibration,'\t',24);
g = 9.81; %Gravitational Constant - m/s^2
con = 0.95;
con = con + ((1 - con)/2);
```

Testing Lift or Drag Consideration

```
if L_or_D == 'L'
    Vcol = 5;
    test = 'Lift';
    Mcol = 3;
elseif L_or_D == 'D'
    Vcol = 7;
    test = 'Drag';
    Mcol = 4;
end
```

Organization of Data

```
V_data = data.data(:,Vcol); %Voltage data - V
M = data.data(:,Mcol); %Mass data - g
M = M(1);
F = g*M/1000; %Force data - N
Run = data.data(:,2); %Run #
```

Gathering Number of Points Used

```
n = 1;
for i = 2:length(Run)
    if Run(i) > Run(i-1)
        n = n + 1;
    end
end
clearvars i
```

Finding Index of Run Change

```
d_r = ones(n+1,1);
d_r(end) = length(Run);
c = 2; %index of force change vector
for i = 2:length(Run)
    if Run(i) > Run(i-1)
        d_r(c) = i;
        c = c + 1;
    end
end
clearvars i
```

Gathering and Taking Mean and Stats of Each Sample

```
V = zeros(n,1);
V_std = V;
N = V;
for i = 1:n
    V(i) = mean(V_data(d_r(i):d_r(i+1)));
    V_std(i) = std(V_data(d_r(i):d_r(i+1)));
    N(i) = d_r(i+1)-d_r(i);
end
clearvars i
```

Calculation of 95 Confidence of Each Sample

```
t_V = tinv(con,N-1);
err_V = t_V.*V_std./sqrt(N);
```

Calculation of Statistical Analysis of Means

```
V_m = mean(V)*ones(n,1);
V_m_std = std(V);
t_m = tinv(con,n-1);
V_m_pop_u = V_m + t_m*V_m_std/sqrt(n);
V_m_pop_b = V_m - t_m*V_m_std/sqrt(n);
```

Plotting Consistency Results

```
figure
hold on
eb = errorbar(1:n,V,err_V,'vertical','ko');
m = plot(1:n,V_m,'g');
pt = plot(1:n,V_m_pop_u,'r--');
pl = plot(1:n,V_m_pop_b,'r--');
title(['Statistical Multiple Weight Measurements for ',num2str(F),' N in ',test,' Direction'],'fontsize',18)
xlabel('Measurement of Weight','fontsize',16)
ylabel('Voltage (V)','fontsize',16)
set(gca,'fontsize',14)
legend([eb,m,pt],{'Sample Analysis','Mean of Sample Average','Population Mean Bounds'})
hold off
```

```
end
```

```
function [L0,D0] = HiCaT_Zero_Cali(File)
```

Data Input

```
data = importdata(File,'\t',24);
```

Calculation of Mean Value of Lift and Drag Voltages

```
L0 = mean(data.data(:,5));
display(['Lift Voltage Zero: ' num2str(L0) ' V']);
D0 = mean(data.data(:,7));
display(['Drag Voltage Zero: ' num2str(D0) ' V']);
```

```
end
```

```
function [sens,zero] = HiCaT_LD_Cali(L_or_D,Calibration)
```

Data Input

```
data = importdata(Calibration,'\t',24);
g = 9.81; %Gravitational Constant - m/s^2
```

Testing Lift or Drag Consideration

```
if L_or_D == 'L'
    Vcol = 5;
    test = 'Lift';
    Mcol = 3;
elseif L_or_D == 'D'
    Vcol = 7;
    test = 'Drag';
    Mcol = 4;
end
```

Organization of Data

```
V_data = data.data(:,Vcol); %Voltage data - V
M = data.data(:,Mcol); %Mass data - g
F_data = g*M/1000; %Force data - N
Run = data.data(:,2); %Run #
```

Gathering Number of Points Used

```
n = 1;
for i = 2:length(Run)
    if Run(i) > Run(i-1)
        n = n + 1;
    end
end
clearvars i
```

Initialization of Run and Mass Change Indices

```
d_F = ones(n,1);
d_F(end) = length(F_data);
d_r = ones(n,1);
c = 1; %index of force change vector
cc = 2; %index of run change vector
for i = 2:length(Run)
    if F_data(i) > F_data(i-1)
        d_F(c) = i;
        c = c + 1;
    end
    if Run(i) > Run(i-1)
        d_r(cc) = i;
        cc = cc + 1;
    end
```

```
end
clearvars i
```

Initialization of Force and Voltage Point Vectors

```
F = zeros(length(n),1);
V = F;
N = V;
for i = 1:n
    F(i) = F_data(d_F(i)-1);
    V(i) = mean(V_data(d_r(i):d_F(i)-1));
    N = d_F(i)-d_r(i);
end
clearvars i
```

Calculation of best fit and 95 confidence for fit and measurement

```
%Best Fit
coeff = polyfit(F,V,1);
m = coeff(1); %V/N
sens = m^-1; %N/V
b = coeff(2); %V
zero = b; %V
V_fit = m*F+b;

%Confidence of Fit
s_VF = sqrt(sum((V-V_fit).^2)/(n-2)); %Standard Deviation
s_VF_pop = s_VF/sqrt(n); %Population Standard Deviation
t = tinv(.975,n-2); %t-Score for linear fit
fit_con_95 = t*s_VF*(1/n + (F-mean(F)).^2/sum((F-mean(F)).^2)).^0.5;
V_fit_u = V_fit + fit_con_95;
V_fit_b = V_fit - fit_con_95;

%Confidence of Measurement
meas_con_95 = t*s_VF*(1 + 1/N + (F-mean(F)).^2/sum((F-mean(F)).^2)).^0.5;
V_meas_u = V_fit + meas_con_95;
V_meas_b = V_fit - meas_con_95;
```

Plotting of data, Range of Possible Population Mean, Best Fit, and Confidences

```
figure
hold on
bf = plot(F,V_fit,'r','linewidth',2); %Best Fit
fc1 = plot(F,V_fit_u,'g','linewidth',2);
fc2 = plot(F,V_fit_b,'g','linewidth',2); %Fit Confidence
mc1 = plot(F,V_meas_u,'m', 'linewidth',2);
mc2 = plot(F,V_meas_b,'m','linewidth',2); %Measurement Confidence
d = plot(F,V,'ko','markerfacecolor','k','markersize',4,'linewidth',2); %Data
title(['95% Confidence for Best Fit and Measurements of ' test ' Calibration'],'fontsize',18)
xlabel('Force (N)','fontsize',16)
ylabel('Voltage (V)','fontsize',16)
set(gca,'fontsize',14)
legend([d,bf,fc1,mc1],{'Mean Data','Linear Regression','Confidence of Regression','Confidence of Measurement'},
'location', 'southeast')
slope = strcat(test,' Sensitivity: ',' ',num2str(sens),' N/V');
text(F(3),V(end-1),slope,'fontsize',14)
yint = strcat(test,' Zero Voltage: ',' ',num2str(b),' V');
text(F(3),V(end-2),yint,'fontsize',14)
hold off
```

```
end
```

Analytical Results Matlab

Data

```
A = importdata('2016 11 13 End Cap.lvm','\t',24);
B = A.data(3:end,:).*1000;
clear vars A

A = importdata('2016 11 28 Zero End Cap.lvm','\t',24);
VLzero = mean(A.data(:,5));
clear vars A

ml = 849332.3048;
bl = -1.2671E-4;
md = 490500;
bd = -6.39E-4;
```

Finding CL and CD

```
AoA = B(:,3);
VL = B(:,5)- VLzero;
VD = B(:,7);

L = -ml*VL; %N
D = md*(VD - bd); %N

rho = 1000; %density in kg/m^3
s = 3.0*0.0254; %m
l = 3.125*0.0254;%m
A = l*s; %m^2
v = 5; % m/s  @ 528 RPM

CL = 2.*(L)./(rho*(v^2)*A)+0.04;
CD = 2.*(D)./(rho*(v^2)*A);

[~,n(1,:)] = min(AoA);
[~,n(2,:)] = min(abs(AoA-3));
[~,n(3,:)] = min(abs(AoA-6));
[~,n(4,:)] = min(abs(AoA-9));
[~,n(5,:)] = min(abs(AoA-12));

ClCd = zeros(1,5);
ClCd(1) = mean(CL(1:n(1))./CD(1:n(1)));
for i=2:4
    ClCd(i) = mean(CL(n(i):n(i+1)-1)./CD(n(i):n(i+1)-1));
end
ClCd(5) = mean(CL(n(5):end)./CD(n(5):end));

figure
plot(AoA,CL,'o')
ylabel('C_L')
xlabel('Angle of Attack (degrees)')
title('End Cap Wingtip')
xticks(0:3:12)


figure
plot(AoA,CD,'o')
ylabel('C_D')
xlabel('Angle of Attack (degrees)')
title('End Cap Wingtip')
xticks(0:3:12)

figure
plot(AoA,CL./CD,'o')
ylabel('C_L/C_D')
xlabel('Angle of Attack (degrees)')
title('End Cap Wingtip')
```

```
xticks(0:3:12)

figure
plot(0:3:12,ClCd,'b-o')
ylabel('C_L/C_D')
xlabel('Angle of Attack (degrees)')
title('End Cap Wingtip')
xticks(0:3:12)
```

Tunnel Parameters

```
P = 95e3; % Pa
T = 293; % K
V = 5; % m/s - at 528 rpm

% Basic Dimensions and constants
nu = 1.004e-6; % m^2/s - dynamic viscosity
rho = 997; % kg/m^3

% Foil Dimensions - Base foil + endcap
S = 3.74 * 0.0254; % m - span
c = 3.125 * 0.0254; % m - chord

% Aspect Ratio
AR = (S^2)/(S*c);

% Reynolds Number
Re = V*c / nu;
```

Load XFOIL Data

```
load('Ellipse1_Re395k.dat')
alpha = Ellipse1_Re395k(6:14,1);
c_l = Ellipse1_Re395k(6:14,2);
c_d = Ellipse1_Re395k(6:14,3);
ratio = (c_l./c_d);
```

Plot c_l/c_d for 2-D Polar

```
figure('Name', '2-D Polars from XFOIL')
plot(alpha,ratio)
title('2-D Polars for Elliptical Airfoil')
xlabel('Angle of Attack, \alpha (deg)')
ylabel('c_l/c_d')
axis([0 12 -0.1 20])

fit = polyfit(alpha,ratio,3);
ratio_2D = fit(1).*alpha.^3 + fit(2).*alpha.^2 + fit(3).*alpha + fit(4);
hold on
plot(alpha,ratio_2D)
legend('Re = 395k','3^{rd} Order Fit','Location','southeast')
```

3-D Effects

```
L = 0.5*rho*(V^2)*S*c.*c_l; % (N) Lift force as a fn of AoA
gamma_o = (4.*L)./(rho*V*S*pi); % Circulation at wing base

y = [0:0.01:S/2];
gamma = gamma_o*sqrt(1-(2*y/S).^2);
figure('Name','Spanwise Circulation')
plot(y,gamma)
title('Elliptical Circulation Distriution Over Finite Foil')
```

```
legend('\alpha = -3','\alpha = 0','\alpha = 3','\alpha = 4','\alpha = 5',...
    '\alpha = 7','\alpha = 8','\alpha = 11','\alpha = 12')
xlabel('y_{spanwise} (m)')
ylabel('\Gamma')

% Downwash (induced downward velocity)
w = -gamma_o/(2*S);

% Induced angle of attack
alpha_i = w/V;

% 3-D Effective Alpha
alpha_3d = alpha+alpha_i;
```

Calculating C_d and C_l including 3-D Effects

```
D_i = (L./S).^2 ./(0.5*rho*(V^2)*pi);
cd_i = D_i ./ (0.5*rho*(V^2)*S);
C_d = (c_l./ratio_2D) + cd_i;
C_d(2) = c_d(2); % No induced drag at 0 degrees

C_l = -alpha_i*pi*AR
ratio_3d = C_l./C_d;
ratio_3d(2) = 0;

%CL_CD_EndCap2016_11_13

figure('Name','C_l/C_d 3D')
plot(alpha,ratio_3d,'bo-',alpha,ratio_2D,'rd-',0:3:12,ClCd,'k^-')
title('C_l/C_d Comparison')
xlabel('\alpha (deg)')
ylabel('C_l/C_d')
grid on
legend('3-D Effects','2-D','Experimental','Location','northwest')
axis([0 12 0 20])

Cd = zeros(1,5);
Cd(1) = mean(CD(1:n(1)));
for i=2:4
    Cd(i) = mean(CD(n(i):n(i+1)-1));
end
Cd(5) = mean(CD(n(5):end));
```

Cavitation Data Analysis Matlab

Calculating Mean Values of Inception Data

```
%All Inception End
PI_mod = P_I(1:18,:);
DI_mod = D_I(1:18,:);
I.all.all = (PI_mod+DI_mod)/2;

%Possible End
I.pos.all = P_I(1:18,:);

%100% End
I.def.all = D_I(1:18,:);

%Low End
PI_mod = [P_I(3:5,:);P_I(8:10,:);P_I(13:15,:);P_I(18,:)];
DI_mod = [D_I(3:5,:);D_I(8:10,:);D_I(13:15,:);D_I(18,:)];
I.all.lre = (PI_mod+DI_mod)/2;

%High End
PI_mod = [P_I(1:2,:);P_I(6:7,:);P_I(11:12,:);P_I(16:17,:)];
DI_mod = [D_I(1:2,:);D_I(6:7,:);D_I(11:12,:);P_I(16:17,:)];
I.all.hre = (PI_mod+DI_mod)/2;

%0/4 End
PI_mod = P_I(11:18,:);
DI_mod = D_I(11:18,:);
I.all.laoa = (PI_mod+DI_mod)/2;

%8/12 End
PI_mod = P_I(1:10,:);
DI_mod = D_I(1:10,:);
I.all.haoa = (PI_mod+DI_mod)/2;

%100% High End
I.def.hre = [D_I(1:2,:);D_I(6:7,:);D_I(11:12,:);P_I(16:17,:)];

%100% Low End
I.def.lre = [D_I(3:5,:);D_I(8:10,:);D_I(13:15,:);D_I(18,:)];

%100% 0/4 End
I.def.laoa = D_I(11:18,:);

%100% 8/12 End
I.def.haoa = D_I(1:10,:);

%Possible Low End
I.pos.lre = [P_I(3:5,:);P_I(8:10,:);P_I(13:15,:);P_I(18,:)];

%Possible High End
I.pos.hre = [P_I(1:2,:);P_I(6:7,:);P_I(11:12,:);P_I(16:17,:)];

%Possible 0/4 End
I.pos.laoa = P_I(11:18,:);

%Possible 8/12 End
I.pos.haoa = P_I(1:10,:);
```

General

```
%All Inception General
PI_mod = [P_I(1:9,:);P_I(11:14,:);P_I(16,:)];
DI_mod = [D_I(1:9,:);D_I(11:14,:);D_I(16,:)];
I.all.all = (PI_mod+DI_mod)/2;

%100% General
I.def.all = [D_I(1:9,:);D_I(11:14,:);D_I(16,:)];
```

```
%Possible General
I.pos.all = [P_I(1:9,:);P_I(11:14,:);P_I(16,:)];

%Low General
PI_mod = [P_I(3:5,:);P_I(8:9,:);P_I(13:14,:)];
DI_mod = [D_I(3:5,:);D_I(8:9,:);D_I(13:14,:)];
I.all.lre = (PI_mod+DI_mod)/2;

%High General
PI_mod = [P_I(1:2,:);P_I(6:7,:);P_I(11:12,:);P_I(16,:)];
DI_mod = [D_I(1:2,:);D_I(6:7,:);D_I(11:12,:);P_I(16,:)];
I.all.hre = (PI_mod+DI_mod)/2;

%0/4 General
PI_mod = P_I(11:18,:);
DI_mod = D_I(11:18,:);
I.all.laoa = (PI_mod+DI_mod)/2;

%8/12 General
PI_mod = P_I(1:10,:);
DI_mod = D_I(1:10,:);
I.all.haoa = (PI_mod+DI_mod)/2;

%100% Low General
I.def.lre = [D_I(3:5,:);D_I(8:9,:);D_I(13:14,:)];

%100% High General
I.def.hre = [D_I(1:2,:);D_I(6:7,:);D_I(11:12,:);P_I(16,:)];

%100% 0/4 General
I.def.laoa = D_I(11:18,:);

%100% 8/12 General
I.def.haoa = D_I(1:10,:);

%Possible Low General
I.pos.lre = [P_I(3:5,:);P_I(8:9,:);P_I(13:14,:)];

%Possible High General
I.pos.hre = [P_I(1:2,:);P_I(6:7,:);P_I(11:12,:);P_I(16,:)];

%Possible 0/4 General
I.pos.laoa = P_I(11:18,:);

%Possible 8/12 General
I.pos.haoa = P_I(1:10,:);
```

Cavitation Inception and Desonance Curves

Wingtips 2016/17

```
clear all; close all; clc
```

Loading Calculated Data

```
data = xlsread('Raw Data - End Cap Cavitation','End Cap - Calculations','A3:W82');
cav_data = [data(:,1:3),data(:,19:23)];
P_I = cav_data(1:4:end,:);
D_I = cav_data(2:4:end,:);
P_D = cav_data(3:4:end,:);
D_D = cav_data(4:4:end,:);
```

Calculating Mean Values of Inception Data

```
%All Inception Angle General
I_12 = [P_I(1:5,:);D_I(1:5,:)];
I_8 = [P_I(6:10,:);D_I(6:10,:)];
I_4 = [P_I(11:15,:);D_I(11:15,:)];
I_0 = [P_I(16:18,:);D_I(16:18,:)];

All Inception General
PI_mod = [P_I(1:9,:);P_I(11:14,:);P_I(16,:)];
DI_mod = [D_I(1:9,:);D_I(11:14,:);D_I(16,:)];
I.all.all = (PI_mod+DI_mod)/2;

%100% General
I.def.all = [D_I(1:9,:);D_I(11:14,:);D_I(16,:)];

%Possible General
I.pos.all = [P_I(1:9,:);P_I(11:14,:);P_I(16,:)];

%Low General
PI_mod = [P_I(3:5,:);P_I(8:9,:);P_I(13:14,:)];
DI_mod = [D_I(3:5,:);D_I(8:9,:);D_I(13:14,:)];
I.all.lre = (PI_mod+DI_mod)/2;

%High General
PI_mod = [P_I(1:2,:);P_I(6:7,:);P_I(11:12,:);P_I(16,:)];
DI_mod = [D_I(1:2,:);D_I(6:7,:);D_I(11:12,:);P_I(16,:)];
I.all.hre = (PI_mod+DI_mod)/2;

%0/4 General
PI_mod = P_I(11:18,:);
DI_mod = D_I(11:18,:);
I.all.laoa = (PI_mod+DI_mod)/2;

%8/12 General
PI_mod = P_I(1:10,:);
DI_mod = D_I(1:10,:);
I.all.haoa = (PI_mod+DI_mod)/2;

%100% Low General
I.def.lre = [D_I(3:5,:);D_I(8:9,:);D_I(13:14,:)];

%100% High General
I = [D_I(1:2,:);D_I(6:7,:);D_I(11:12,:)];

%100% 0/4 General
I.def.laoa = D_I(11:18,:);

%100% 8/12 General
I.def.haoa = D_I(1:10,:);

%Possible Low General
I.pos.lre = [P_I(3:5,:);P_I(8:9,:);P_I(13:14,:)];

%Possible High General
I.pos.hre = [P_I(1:2,:);P_I(6:7,:);P_I(11:12,:);P_I(16,:)];

%Possible 0/4 General
I.pos.laoa = P_I(11:18,:);

%Possible 8/12 General
I.pos.haoa = P_I(1:10,:);
```

Calculation of Ideal Exponents

```
r2 = zeros(length(-3:0.1:3),length(-3:0.1:3),length(-3:0.1:3));
r2_b0 = zeros(length(-3:0.01:3),length(-3:0.01:-3));
r2_a2 = zeros(length(-3:0.05:3),length(-3:0.05:-3));
```

```
r2_a2b0 = zeros(length(-3:0.01:3),1);
r2_c04 = zeros(length(-3:0.05:3),length(-3:0.05:-3));
r2_c04b0 = zeros(length(-3:0.01:3),1);
r2_a1 = zeros(length(-3:0.05:3),length(-3:0.05:-3));
r2_a1b0 = zeros(length(-3:0.01:3),1);

%(a,b,c) = (a,b,c)
i = 1;
for a = -3:0.1:3
    j=1;
    for b = -3:0.1:3
        k=1;
        for c = -3:0.1:3
            x = I(:,4).^a.*I(:,5).^b.*I(:,8).^c;
            p = polyfitZero(x,I(:,7),1);
            mdl = polyval(p,x);
            r2(i,j,k) = 1-sum((I(:,7)-mdl).^2)/sum((I(:,7)-mean(I(:,7))).^2);
            clearvars x poly mdl
            k = k+1;
        end
        j = j+1;
    end
    i = i+1;
end
clearvars a b c i j k

%(a,b,c) = (a,0,c)
i = 1;
b = 0;
for a = -3:0.01:3
    j = 1;
    for c = -3:0.01:3
         x = I(:,4).^a.*I(:,5).^b.*I(:,8).^c;
         p = polyfitZero(x,I(:,7),1);
         mdl = polyval(p,x);
         r2_b0(i,j) = 1-sum((I(:,7)-mdl).^2)/sum((I(:,7)-mean(I(:,7))).^2);
         clearvars x poly mdl
         j = j+1;
    end
    i = i+1;
end
clearvars a b c i j

%(a,b,c) = (2,b,c)
a = 2;
i = 1;
for b = -3:0.05:3
    j = 1;
    for c = -3:0.5:3
        x = I(:,4).^a.*I(:,5).^b.*I(:,8).^c;
        p = polyfitZero(x,I(:,7),1);
        mdl = polyval(p,x);
        r2_a2(i,j) = 1-sum((I(:,7)-mdl).^2)/sum((I(:,7)-mean(I(:,7))).^2);
        clearvars x poly mdl
        j = j+1;
    end
    i = i+1;
end
clearvars a b c i j

%(a,b,c) = (2,0,c)
a = 2;
b = 0;
i = 1;
for c = -3:0.01:3
    x = I(:,4).^a.*I(:,5).^b.*I(:,8).^c;
    p = polyfitZero(x,I(:,7),1);
    mdl = polyval(p,x);
    r2_a2b0(i) = 1-sum((I(:,7)-mdl).^2)/sum((I(:,7)-mean(I(:,7))).^2);
    clearvars x poly mdl
    i = i+1;
end
```

```
clearvars a b c i

%(a,b,c) = (1,b,c)
a = 1;
i = 1;
for b = -3:0.05:3
    j = 1;
    for c = -3:0.5:3
        x = I(:,4).^a.*I(:,5).^b.*I(:,8).^c;
        p = polyfitZero(x,I(:,7),1);
        mdl = polyval(p,x);
        r2_a1(i,j) = 1-sum((I(:,7)-mdl).^2)/sum((I(:,7)-mean(I(:,7))).^2);
        clearvars x poly mdl
        j = j+1;
    end
    i = i+1;
end
clearvars a b c i j

%(a,b,c) = (1,0,c)
a = 1;
b = 0;
i = 1;
for c = -3:0.01:3
    x = I(:,4).^a.*I(:,5).^b.*I(:,8).^c;
    p = polyfitZero(x,I(:,7),1);
    mdl = polyval(p,x);
    r2_a1b0(i) = 1-sum((I(:,7)-mdl).^2)/sum((I(:,7)-mean(I(:,7))).^2);
    clearvars x poly mdl
    i = i+1;
end
clearvars a b c i

%(a,b,c) = (a,b,0.4)
c = 0.4;
i = 1;
for a = -3:0.05:3
    j = 1;
    for b = -3:0.5:3
        x = I(:,4).^a.*I(:,5).^b.*I(:,8).^c;
        p = polyfitZero(x,I(:,7),1);
        mdl = polyval(p,x);
        r2_c04(i,j) = 1-sum((I(:,7)-mdl).^2)/sum((I(:,7)-mean(I(:,7))).^2);
        clearvars x poly mdl
        j = j+1;
    end
    i = i+1;
end
clearvars a b c i j

%(a,b,c) = (a,0,0.4)
b = 0;
c = 0.4;
i = 1;
for a = -3:0.01:3
    x = I(:,4).^a.*I(:,5).^b.*I(:,8).^c;
    p = polyfitZero(x,I(:,7),1);
    mdl = polyval(p,x);
    r2_c04b0(i) = 1-sum((I(:,7)-mdl).^2)/sum((I(:,7)-mean(I(:,7))).^2);
    clearvars x poly mdl
    i = i+1;
end
clearvars a b c i
```

Finding Ideal Exponents

```
[r2_max,ind] = max(r2(:));
[A,B,C] = ind2sub([length(-3:0.1:3),length(-3:0.1:3),length(-3:0.1:3)],ind);
[r2_b0_max,ind_b0] = max(r2_b0(:));
```

```
[A0,B0,C0] = ind2sub([length(-3:0.01:3),length(-3:0.01:3)],ind_b0);
[r2_a2_max,ind_a2] = max(r2_a2(:));
[Ba2,Ca2] = ind2sub([length(-3:0.05:3),length(-3:0.05:3)],ind_a2);
[r2_a2b0_max,ind_a2b0] = max(r2_a2b0(:));
[Ca2b0] = ind2sub([length(-3:0.01:3),1],ind_a2b0);
[r2_a1_max,ind_a1] = max(r2_a1(:));
[Ba1,Ca1] = ind2sub([length(-3:0.05:3),length(-3:0.05:3)],ind_a1);
[r2_a1b0_max,ind_a1b0] = max(r2_a1b0(:));
[Ca1b0] = ind2sub([length(-3:0.01:3),1],ind_a1b0);
[r2_c04_max,ind_c04] = max(r2_c04(:));
[Ac04,Bc04] = ind2sub([length(-3:0.05:3),length(-3:0.05:3)],ind_c04);
[r2_c04b0_max,ind_c04b0] = max(r2_c04b0(:));
[Ac04b0] = ind2sub([length(-3:0.01:3),1],ind_c04b0);

a_ideal = 0.1*(A-1)-3;
b_ideal = 0.1*(B-1)-3;
c_ideal = 0.1*(C-1)-3;
a_b0 = 0.01*(A0-1)-3;
b_b0 = 0;
c_b0 = 0.01*(B0-1)-3;
a_1 = 1;
b_1 = 1;
c_1 = 1;
a_a2 = 2;
b_a2 = 0.05*(Ba2-1)-3;
c_a2 = 0.05*(Ca2-1)-3;
a_a2b0 = 2;
b_a2b0 = 0;
a_a1 = 1;
b_a1 = 0.05*(Ba1-1)-3;
c_a1 = 0.05*(Ca1-1)-3;
a_a1b0 = 1;
b_a1b0 = 0;
c_a1b0 = 0.01*(Ca1b0-1)-3;
c_a2b0 = 0.01*(Ca2b0-1)-3;
a_c04 = 0.05*(Ac04-1)-3;
b_c04 = 0.05*(Ac04-1)-3;
c_c04 = 0.4;
a_c04b0 = 0.01*(Ac04b0-1)-3;
b_c04b0 = 0;
c_c04b0 = 0.4;
```

Calculation of Best Fit

```
tran_MI = I(:,4).^a_ideal.*I(:,5).^b_ideal.*I(:,8).^c_ideal;
tran_PI = PI_mod(:,4).^a_ideal.*PI_mod(:,5).^b_ideal.*PI_mod(:,8).^c_ideal;
tran_DI = DI_mod(:,4).^a_ideal.*DI_mod(:,5).^b_ideal.*DI_mod(:,8).^c_ideal;
Arndt_MI = I(:,4).^2.*I(:,8).^0.4;
Arndt_PI = PI_mod(:,4).^2.*PI_mod(:,8).^0.4;
Arndt_DI = DI_mod(:,4).^2.*DI_mod(:,8).^0.4;
b0_MI = I(:,4).^a_b0.*I(:,8).^c_b0;
b0_PI = PI_mod(:,4).^a_b0.*PI_mod(:,8).^c_b0;
b0_DI = DI_mod(:,4).^a_b0.*DI_mod(:,8).^c_b0;
all1_MI = I(:,4).^a_1.*I(:,5).^b_1.*I(:,8).^c_1;
all1_b0_MI = I(:,4).^a_1.*I(:,8).^c_1;
a2_MI = I(:,4).^2.*I(:,5).^b_a2.*I(:,8).^c_a2;
a2b0_MI = I(:,4).^2.*I(:,8).^c_a2b0;
a1_MI = I(:,4).*I(:,5).^b_a1.*I(:,8).^c_a1;
a1b0_MI = I(:,4).*I(:,8).^c_a1b0;
c04_MI = I(:,4).^a_c04.*I(:,5).^b_c04.*I(:,8).^0.4;
c04b0_MI = I(:,4).^a_c04b0.*I(:,8).^0.4;
poly_I = polyfitZero(tran_MI,I(:,7),1);
poly_A = polyfitZero(Arndt_MI,I(:,7),1);
poly_b0 = polyfitZero(b0_MI,I(:,7),1);
poly_a2 = polyfitZero(a2_MI,I(:,7),1);
poly_a2b0 = polyfitZero(a2b0_MI,I(:,7),1);
poly_a1 = polyfitZero(a1_MI,I(:,7),1);
poly_a1b0 = polyfitZero(a1b0_MI,I(:,7),1);
poly_c04 = polyfitZero(c04_MI,I(:,7),1);
```

```
poly_c04b0 = polyfitZero(c04b0_MI,I(:,7),1);
x1 = 0:max(tran_MI)/(length(I(:,7))-1):max(tran_MI);
x2 = 0:max(Arndt_MI)/(length(I(:,7))-1):max(Arndt_MI);
x3 = 0:max(b0_MI)/(length(I(:,7))-1):max(b0_MI);
x4 = 0:max(a2_MI)/(length(I(:,7))-1):max(a2_MI);
x5 = 0:max(a2b0_MI)/(length(I(:,7))-1):max(a2b0_MI);
x6 = 0:max(c04_MI)/(length(I(:,7))-1):max(c04_MI);
x7 = 0:max(c04b0_MI)/(length(I(:,7))-1):max(c04b0_MI);
x8 = 0:max(a1_MI)/(length(I(:,7))-1):max(a1_MI);
x9 = 0:max(a1b0_MI)/(length(I(:,7))-1):max(a1b0_MI);
Cav_fit = polyval(poly_I,x1);
Arndt_fit = polyval(poly_A,x2);
b0_fit = polyval(poly_b0,x3);
a2_fit = polyval(poly_a2,x4);
a2b0_fit = polyval(poly_a2b0,x5);
c04_fit = polyval(poly_c04,x6);
c04b0_fit = polyval(poly_c04b0,x7);
a1_fit = polyval(poly_a1,x8);
a1b0_fit = polyval(poly_a1b0,x9);
r2_Ideal = r2_max;
r2_b0 = r2_b0_max;
r2_a2 = r2_a2_max;
r2_a2b0 = r2_a2b0_max;
r2_c04 = r2_c04_max;
r2_c04b0 = r2_c04b0_max;
r2_a1 = r2_a1_max;
r2_a1b0 = r2_a1b0_max;
r2_Arndt = 1-sum((I(:,7)'-Arndt_fit).^2)/sum((I(:,7)-mean(I(:,7))).^2);
```

Calculating Error Bars for Mean Inception Data

```
cav_errorp = PI_mod(:,7) - I(:,7);
cav_errorn = I(:,7) - DI_mod(:,7);
tran_errorp = tran_PI - tran_MI;
tran_errorn = tran_MI - tran_DI;
Arndt_errorp = Arndt_PI - Arndt_MI;
Arndt_errorn = Arndt_MI - Arndt_DI;
b0_errorp = b0_PI - b0_MI;
b0_errorn = b0_MI - b0_DI;
CL_errorp = PI_mod(:,4) - I(:,4);
CL_errorn = I(:,4) - DI_mod(:,4);
CD_errorp = PI_mod(:,5) - I(:,5);
CD_errorn = I(:,5) - DI_mod(:,5);
Re_errorp = PI_mod(:,8) - I(:,8);
Re_errorn = I(:,8) - DI_mod(:,8);
```

Plotting of Cavitation Inception Curves

```
figure('color',[1,1,1])
subplot(2,2,1)
hold on
plot(I_0(:,4),I_0(:,7),'ko','markerfacecolor','r','markersize',6)
plot(I_4(:,4),I_4(:,7),'ko','markerfacecolor','b','markersize',6)
plot(I_8(:,4),I_8(:,7),'ko','markerfacecolor','g','markersize',6)
plot(I_12(:,4),I_12(:,7),'ko','markerfacecolor','m','markersize',6)
xlabel('C_L','fontsize',16)
ylabel('\sigma','fontsize',16)
set(gca,'fontsize',14)
grid on
box on
hold off
subplot(2,2,2)
hold on
plot(I_0(:,5),I_0(:,7),'ko','markerfacecolor','r','markersize',6)
plot(I_4(:,5),I_4(:,7),'ko','markerfacecolor','b','markersize',6)
plot(I_8(:,5),I_8(:,7),'ko','markerfacecolor','g','markersize',6)
plot(I_12(:,5),I_12(:,7),'ko','markerfacecolor','m','markersize',6)
```

```
xlabel('C_D','fontsize',16)
ylabel('\sigma','fontsize',16)
set(gca,'fontsize',14)
grid on
box on
hold off
subplot(2,2,3)
hold on
plot(I_0(:,8)/1000,I_0(:,7),'ko','markerfacecolor','r','markersize',6)
plot(I_4(:,8)/1000,I_4(:,7),'ko','markerfacecolor','b','markersize',6)
plot(I_8(:,8)/1000,I_8(:,7),'ko','markerfacecolor','g','markersize',6)
plot(I_12(:,8)/1000,I_12(:,7),'ko','markerfacecolor','m','markersize',6)
xlabel('(10^3) Re','fontsize',16)
ylabel('\sigma','fontsize',16)
set(gca,'fontsize',14)
grid on
box on
hold off
subplot(2,2,4)
hold on
plot(I_0(:,2),I_0(:,7),'ko','markerfacecolor','r','markersize',6)
plot(I_4(:,2),I_4(:,7),'ko','markerfacecolor','b','markersize',6)
plot(I_8(:,2),I_8(:,7),'ko','markerfacecolor','g','markersize',6)
plot(I_12(:,2),I_12(:,7),'ko','markerfacecolor','m','markersize',6)
xlabel('AoA (\circ)','fontsize',16)
ylabel('\sigma','fontsize',16)
set(gca,'fontsize',14)
grid on
box on
legend('AoA=0\circ','AoA=4\circ','AoA=8\circ','AoA=12\circ')
hold off
mtit('End Cap Tip Cavitation Profiles','fontsize',18)

figure('color',[31/255 78/255 121/255])
hold on
plot(x1,Cav_fit,'k--','linewidth',2)
plot(tran_MI,I(:,7),'ko','markerfacecolor','r','markersize',6)
conv_xlab = strcat('C_L^{',num2str(a_ideal),'}C_D^{',num2str(b_ideal),'}Re^{',num2str(c_ideal),'}');
title(strcat('\sigma=K',conv_xlab),'fontsize',18,'color','w')
xlabel(conv_xlab,'fontsize',16,'color','w')
ylabel('\sigma','fontsize',16,'color','w')
set(gca,'fontsize',14)
set(gca,'xcolor','w')
set(gca,'ycolor','w')
set(gca,'gridcolor','k')
legend(strcat('Linear Regression: K=',num2str(round(poly_I(1),-11)/10^11),'(10^{11})'),'Data')
grid on
box on
hold off

figure('color',[1,1,1])
hold on
plot(x3,b0_fit,'k--','linewidth',2)
plot(b0_MI,I(:,7),'ko','markerfacecolor','r','markersize',6)
conv_b0_xlab = strcat('C_L^{',num2str(a_b0),'}Re^{',num2str(c_b0),'}');
title('Optimized Linear Fit for General Tip Cavitation','fontsize',18)
xlabel(conv_b0_xlab,'fontsize',16)
ylabel('\sigma','fontsize',16)
set(gca,'fontsize',14)
legend(strcat('Linear Regression: K=',num2str(round(poly_b0(1),-9)/10^9),'(10^{9})'),'Data')
grid on
box on
hold off

figure('color',[31/255 78/255 121/255])
hold on
plot(x2,Arndt_fit,'k--','linewidth',2)
plot(Arndt_MI,I(:,7),'ko','markerfacecolor','r','markersize',6)
title('\sigma = KC_L^2Re^{0.4}','fontsize',18,'color','w')
xlabel('C_L^2Re^{0.4}','fontsize',16,'color','w')
ylabel('\sigma','fontsize',16,'color','w')
set(gca,'fontsize',14)
```

```
set(gca,'xcolor','w')
set(gca,'ycolor','w')
set(gca,'gridcolor','k')
legend(strcat('Linear Regression: K=',num2str(round(poly_A(1),3))),'Data')
grid on
box on
hold off

figure('color',[31/255 78/255 121/255])
plot(all1_MI,I(:,7),'ko','markerfacecolor','r','markersize',6)
title(strcat('\sigma=KC_LC_DRe'),'fontsize',18,'color','w')
xlabel('C_LC_DRe','fontsize',16,'color','w')
ylabel('\sigma','fontsize',16,'color','w')
set(gca,'fontsize',14)
set(gca,'xcolor','w')
set(gca,'ycolor','w')
set(gca,'gridcolor','k')
grid on
box on

figure('color',[31/255 78/255 121/255])
plot(all1_b0_MI,I(:,7),'ko','markerfacecolor','r','markersize',6)
title('\sigma=KC_LRe','fontsize',18,'color','w')
xlabel('C_LRe','fontsize',16,'color','w')
ylabel('\sigma','fontsize',16','color','w')
set(gca,'fontsize',14)
set(gca,'xcolor','w')
set(gca,'ycolor','w')
set(gca,'gridcolor','k')
axis([0,5*10^5,0,4])
grid on
box on

figure('color',[31/255 78/255 121/255])
hold on
plot(x4,a2_fit,'k--','linewidth',2)
plot(a2_MI,I(:,7),'ko','markerfacecolor','r','markersize',6)
conv_a2_xlab = strcat('C_L^2C_D^{',num2str(b_a2),'}Re^{',num2str(c_a2),'}');
title(strcat('\sigma=K',conv_a2_xlab),'fontsize',18,'color','w')
xlabel(conv_a2_xlab,'fontsize',16,'color','w')
ylabel('\sigma','fontsize',16,'color','w')
legend(strcat('Linear Regression: K=',num2str(round(poly_a2(1),-14)/10^14),'(10^{14})'),'Data')
set(gca,'fontsize',14)
set(gca,'xcolor','w')
set(gca,'ycolor','w')
set(gca,'gridcolor','k')
grid on
box on
hold off

figure('color',[31/255 78/255 121/255])
hold on
plot(x5,a2b0_fit,'k--','linewidth',2)
plot(a2b0_MI,I(:,7),'ko','markerfacecolor','r','markersize',6)
conv_a2b0_xlab = strcat('C_L^2Re^{',num2str(c_a2b0),'}');
title(strcat('\sigma=K',conv_a2b0_xlab),'fontsize',18,'color','w')
xlabel(conv_a2b0_xlab,'fontsize',16,'color','w')
ylabel('\sigma','fontsize',16,'color','w')
legend(strcat('Linear Regression: K=',num2str(round(poly_a2b0(1),-8)/10^8),'(10^8)'),'Data')
set(gca,'fontsize',14)
set(gca,'xcolor','w')
set(gca,'ycolor','w')
set(gca,'gridcolor','k')
grid on
box on
hold off

figure('color',[31/255 78/255 121/255])
hold on
plot(x8,a1_fit,'k--','linewidth',2)
plot(a1_MI,I(:,7),'ko','markerfacecolor','r','markersize',6)
conv_a1_xlab = strcat('C_LC_D^{',num2str(b_a1),'}Re^{',num2str(c_a1),'}');
```

```
title(strcat('\sigma=K',conv_a1_xlab),'fontsize',18,'color','w')
xlabel(conv_a1_xlab,'fontsize',16,'color','w')
ylabel('\sigma','fontsize',16,'color','w')
legend(strcat('Linear Regression: K=',num2str(round(poly_a1(1),-14)/10^14),'(10^{14})'),'Data')
set(gca,'fontsize',14)
set(gca,'xcolor','w')
set(gca,'ycolor','w')
set(gca,'gridcolor','k')
grid on
box on
hold off

figure('color',[31/255 78/255 121/255])
hold on
plot(x9,a1b0_fit,'k--','linewidth',2)
plot(a1b0_MI,I(:,7),'ko','markerfacecolor','r','markersize',6)
conv_a1b0_xlab = strcat('C_LRe^{',num2str(c_a1b0),'}');
title(strcat('\sigma=K',conv_a1b0_xlab),'fontsize',18,'color','w')
xlabel(conv_a1b0_xlab,'fontsize',16,'color','w')
ylabel('\sigma','fontsize',16,'color','w')
legend(strcat('Linear Regression: K=',num2str(round(poly_a1b0(1),-12)/10^12),'(10^{12})'),'Data')
set(gca,'fontsize',14)
set(gca,'xcolor','w')
set(gca,'ycolor','w')
set(gca,'gridcolor','k')
grid on
box on
hold off

figure('color',[31/255 78/255 121/255])
hold on
plot(x6,c04_fit,'k--','linewidth',2)
plot(c04_MI,I(:,7),'ko','markerfacecolor','r','markersize',6)
conv_c04_xlab = strcat('C_L^{',num2str(a_c04),'}C_D^{',num2str(b_c04),'}Re^{0.4}');
title(strcat('\sigma=K',conv_c04_xlab),'fontsize',18,'color','w')
xlabel(conv_c04_xlab,'fontsize',16,'color','w')
ylabel('\sigma','fontsize',16,'color','w')
legend(strcat('Linear Regression: K=',num2str(round(poly_c04(1),4))),'Data')
set(gca,'fontsize',14)
set(gca,'xcolor','w')
set(gca,'ycolor','w')
set(gca,'gridcolor','k')
grid on
box on
hold off

figure('color',[31/255 78/255 121/255])
hold on
plot(x7,c04b0_fit,'k--','linewidth',2)
plot(c04b0_MI,I(:,7),'ko','markerfacecolor','r','markersize',6)
conv_c04b0_xlab = strcat('C_L^{',num2str(a_c04b0),'}Re^{0.4}');
title(strcat('\sigma=K',conv_c04b0_xlab),'fontsize',18,'color','w')
xlabel(conv_c04b0_xlab,'fontsize',16,'color','w')
ylabel('\sigma','fontsize',16,'color','w')
legend(strcat('Linear Regression: K=',num2str(round(poly_c04b0(1),4))),'Data')
set(gca,'fontsize',14)
set(gca,'xcolor','w')
set(gca,'ycolor','w')
set(gca,'gridcolor','k')
grid on
box on
hold off
```

CL/CD Plot Creation for Cavitation Data

```
close all;
```

Data Input

```
data1 = xlsread('Raw Data - End Cap Cavitation','End Cap - Calculations','A3:W83');
data2 = xlsread('Raw Data - General Cavitation','General - Calculated','A3:W83');
AoA = [12,8,4,0];
```

Seperation of Data for End Cap

```
ec_900 = [mean(data1(1:3,:),1);mean(data1(21:24,:),1);mean(data1(41:44,:),1);mean(data1(61:64,:),1)];
ec_700 = [mean(data1(5:8,:),1);mean(data1(27:28,:),1);mean(data1(45:46,:),1);mean(data1(65:68,:),1)];
ec_500 = [mean(data1(9:12,:),1);mean(data1(31:32,:),1);mean(data1(49:2:51,:),1);mean(data1(69:72,:),1)];
ec_400 = [mean(data1(13:16,:),1);mean(data1(36,:),1);mean(data1(53:56,:),1)];
ec_300 = [mean(data1(19:20,:),1);mean(data1(39:40,:),1);mean(data1(57:60,:),1)];
```

Seperation of Data for General

```
g_900 = [min(data2(3:4,:),[],1);min(data2(24,:),[],1);min(data2(41:44,:),[],1);min(data2(61:64,:),[],1)];
g_700 = [min(data2(5:8,:),[],1);min(data2(28,:),[],1);min(data2(47:48,:),[],1)];
g_500 = [min(data2(9:12,:),[],1);min(data2(29:32,:),[],1);min(data2(53:56,:),[],1)];
g_400 = [min(data2(13:16,:),[],1);min(data2(33:36,:),[],1)];
```

Calculation of Mean Reynolds for Each Speed

```
ec_re900 = round(mean(ec_900(:,end)),-4)/1000;
ec_re700 = round(mean(ec_700(:,end)),-4)/1000;
ec_re500 = round(mean(ec_500(:,end)),-4)/1000;
ec_re400 = round(mean(ec_400(:,end)),-4)/1000;
ec_re300 = round(mean(ec_300(:,end)),-4)/1000;

g_re900 = round(mean(g_900(:,end)),-4)/1000;
g_re700 = round(mean(g_700(:,end)),-4)/1000;
g_re500 = round(mean(g_500(:,end)),-4)/1000;
g_re400 = round(mean(g_400(:,end)),-4)/1000;
```

Plotting Data for End Cap

```
figure('color',[1,1,1])
hold on
plot(ec_900(:,2),ec_900(:,end-2),'ks','markerfacecolor','b')
plot(ec_700(:,2),ec_700(:,end-2),'ko','markerfacecolor','r')
plot(ec_500(:,2),ec_500(:,end-2),'kp','markerfacecolor','g')
plot(ec_400(:,2),ec_400(:,end-2),'kv','markerfacecolor','m')
plot(ec_300(:,2),ec_300(:,end-2),'k^','markerfacecolor','c')
title('End Cap Lift-to-Drag Ratio','fontsize',18')
xlabel('Angle of Attack ({\circ})','fontsize',16)
ylabel('C_L/C_D','fontsize',16)
set(gca,'fontsize',14)
legend(strcat('Re~',num2str(ec_re900),'(10^3)'),strcat('Re~',num2str(ec_re700),'(10^3)'),strcat('Re~',num2str(ec_re500)
,'(10^3)'),strcat('Re~',num2str(ec_re400),'(10^3)'),strcat('Re~',num2str(ec_re300),'(10^3)'))
axis([0,12,0,7])
grid on
box on
hold off

figure('color',[31/255 78/255 121/255])
plot(AoA,[min(data1(19:20,end-2),[],1);min(data1(39:40,end-2),[],1);min(data1(57:60,end-2),[],1);mean(data1(69:72,end-
2),1)],'ko--','markerfacecolor','r')
title(strcat('End Cap Lift-to-Drag Ratio: Re~',num2str(round(ec_re300)),'(10^3)'),'fontsize',18,'color','w')
xlabel('Angle of Attack ({\circ})','fontsize',16,'color','w')
ylabel('C_L/C_D','fontsize',16,'color','w')
set(gca,'fontsize',14)
```

```
set(gca,'xcolor','w')
set(gca,'ycolor','w')
set(gca,'gridcolor','k')
axis([0,12,0,6])
grid on
box on
```

Plotting Data for General

```
figure('color',[1,1,1])
hold on
plot(g_900(:,2),g_900(:,end-2),'ks','markerfacecolor','b')
plot(g_700(:,2),g_700(:,end-2),'ko','markerfacecolor','r')
plot(g_500(:,2),g_500(:,end-2),'kp','markerfacecolor','g')
plot(g_400(:,2),g_400(:,end-2),'kv','markerfacecolor','m')
title('Lift-to-Drag','fontsize',18)
xlabel('Angle of Attack ({\circ})','fontsize',16)
ylabel('C_L/C_D','fontsize',16)
set(gca,'fontsize',14)
legend(strcat('Re~',num2str(g_re900),'(10^3)'),strcat('Re~',num2str(g_re700),'(10^3)'),strcat('Re~',num2str(g_re500),'(
10^3)'),strcat('Re~',num2str(g_re400),'(10^3)'))
grid on
box on
hold off

figure('color',[31/255 78/255 121/255])
hold on
plot(AoA,[g_900(1,end-2);g_500(2,end-2);g_900(3:4,end-2)],'ko--','markerfacecolor','r')
title(strcat('General Lift-to-Drag Ratio: Re~',num2str(round(g_re900)),'(10^3)'),'fontsize',18,'color','w')
xlabel('Angle of Attack ({\circ})','fontsize',16,'color','w')
ylabel('C_L/C_D','fontsize',16,'color','w')
set(gca,'fontsize',14)
set(gca,'xcolor','w')
set(gca,'ycolor','w')
set(gca,'gridcolor','k')
axis([0,12,0,6])
grid on
box on
hold on
```

Combined Plots

```
figure('color',[1,1,1])
hold on
plot(ec_900(:,2),[min(data1(1:3,end-2),[],1);min(data1(21:24,end-2),[],1);min(data1(41:44,end-
2),[],1);min(data1(61:64,end-2),[],1)],'ko--','markerfacecolor','r')
plot(g_900(:,2),g_900(:,end-2),'kv:','markerfacecolor','b')
title('Lift-to-Drag Ratios for Wing Tip Devices','fontsize',18)
xlabel('Angle of Attack ({\circ})','fontsize',16)
ylabel('C_L/C_D','fontsize',16)
set(gca,'fontsize',14)
legend(strcat('End Cap: Re~',num2str(ec_re900),'(10^3)'),strcat('General: Re~',num2str(g_re900),'(10^3)'))
grid on
box on
hold off

figure('color',[31/255 78/255 121/255])
hold on
plot(AoA,[min(data1(19:20,end-2),[],1);min(data1(39:40,end-2),[],1);min(data1(57:60,end-2),[],1);mean(data1(69:72,end-
2),1)],'ko--','markerfacecolor','r')
plot(AoA,[g_900(1,end-2);g_500(2,end-2);g_900(3:4,end-2)],'kv:','markerfacecolor','b')
title('Lift-to-Drag Ratios for Wing Tip Devices','fontsize',18,'color','w')
xlabel('Angle of Attack ({\circ})','fontsize',16,'color','w')
ylabel('C_L/C_D','fontsize',16,'color','w')
set(gca,'fontsize',14)
set(gca,'xcolor','w')
set(gca,'ycolor','w')
```

```
set(gca,'gridcolor','k')
legend(strcat('End Cap: Re~',num2str(round(ec_re300)),'(10^3)'),strcat('General:
Re~',num2str(round(g_re900)),'(10^3)'))
axis([0,12,0,6])
grid on
box on
hold on
```

Cavitation Analysis of Expected Equation

```
clear all; close all; clc
```

Loading Calculated Data

```
data1 = xlsread('Raw Data - General Cavitation','General - Calculated','A3:W82');
data2 = xlsread('Raw Data - End Cap Cavitation','End Cap - Calculations','A3:W82');
data1 = [data1(:,1:3),data1(:,19:23)];
data2 = [data2(:,1:3),data2(:,19:23)];
P_I1 = data1(1:4:end,:);
D_I1 = data1(2:4:end,:);
```

Calculating Mean Values of Inception Data

```
%All Inception General
PI_mod = [P_I1(1:9,:);P_I1(11:14,:);P_I1(16,:)];
DI_mod = [D_I1(1:9,:);D_I1(11:14,:);D_I1(16,:)];
I.all.all = (PI_mod+DI_mod)/2;

%100% General
I.def.all = [D_I1(1:9,:);D_I1(11:14,:);D_I1(16,:)];

%Possible General
I.pos.all = [P_I1(1:9,:);P_I1(11:14,:);P_I1(16,:)];

%Low General
PI_mod = [P_I1(3:5,:);P_I1(8:9,:);P_I1(13:14,:)];
DI_mod = [D_I1(3:5,:);D_I1(8:9,:);D_I1(13:14,:)];
I.all.lre = (PI_mod+DI_mod)/2;

%High General
PI_mod = [P_I1(1:2,:);P_I1(6:7,:);P_I1(11:12,:);P_I1(16,:)];
DI_mod = [D_I1(1:2,:);D_I1(6:7,:);D_I1(11:12,:);P_I1(16,:)];
I.all.hre = (PI_mod+DI_mod)/2;

%0/4 General
PI_mod = P_I1(11:18,:);
DI_mod = D_I1(11:18,:);
I.all.laoa = (PI_mod+DI_mod)/2;

%8/12 General
PI_mod = P_I1(1:10,:);
DI_mod = D_I1(1:10,:);
I.all.haoa = (PI_mod+DI_mod)/2;

%100% Low General
I.def.lre = [D_I1(3:5,:);D_I1(8:9,:);D_I1(13:14,:)];

%100% High General
I_g = [D_I1(1:2,:);D_I1(6:7,:);D_I1(11:12,:);P_I1(16,:)];
I_g = [D_I1(1:2,:);D_I1(6:7,:);D_I1(11:12,:)];

%100% 0/4 General
I.def.laoa = D_I1(11:18,:);

%100% 8/12 General
```

```
I.def.haoa = D_I1(1:10,:);

%Possible Low General
I.pos.lre = [P_I1(3:5,:);P_I1(8:9,:);P_I1(13:14,:)];

%Possible High General
I.pos.hre = [P_I1(1:2,:);P_I1(6:7,:);P_I1(11:12,:);P_I1(16,:)];

%Possible 0/4 General
I.pos.laoa = P_I1(11:18,:);

%Possible 8/12 General
I.pos.haoa = P_I1(1:10,:);

%All Inception End
PI_mod = P_I(1:18,:);
DI_mod = D_I(1:18,:);
I.all.all = (PI_mod+DI_mod)/2;

%Possible End
I.pos.all = P_I(1:18,:);

%100% End
I.def.all = D_I(1:18,:);

%Low End
PI_mod = [P_I(3:5,:);P_I(8:10,:);P_I(13:15,:);P_I(18,:)];
DI_mod = [D_I(3:5,:);D_I(8:10,:);D_I(13:15,:);D_I(18,:)];
I.all.lre = (PI_mod+DI_mod)/2;

%High End
PI_mod = [P_I(1:2,:);P_I(6:7,:);P_I(11:12,:);P_I(16:17,:)];
DI_mod = [D_I(1:2,:);D_I(6:7,:);D_I(11:12,:);P_I(16:17,:)];
I.all.hre = (PI_mod+DI_mod)/2;

%0/4 End
PI_mod = P_I(11:18,:);
DI_mod = D_I(11:18,:);
I.all.laoa = (PI_mod+DI_mod)/2;

%8/12 End
PI_mod = P_I(1:10,:);
DI_mod = D_I(1:10,:);
I.all.haoa = (PI_mod+DI_mod)/2;

100% High End
I.def.hre = [D_I(1:2,:);D_I(6:7,:);D_I(11:12,:);P_I(16:17,:)];
I.def.hre = [D_I(1:2,:);D_I(6:7,:);D_I(11:12,:);P_I(16:17,:)];

%100% Low End
I.def.lre = [D_I(3:5,:);D_I(8:10,:);D_I(13:15,:);D_I(18,:)];

%100% 0/4 End
I.def.laoa = D_I(11:18,:);

%100% 8/12 End
I.def.haoa = D_I(1:10,:);

%Possible Low End
I.pos.lre = [P_I(3:5,:);P_I(8:10,:);P_I(13:15,:);P_I(18,:)];

%Possible High End
I.pos.hre = [P_I(1:2,:);P_I(6:7,:);P_I(11:12,:);P_I(16:17,:)];

%Possible 0/4 End
I.pos.laoa = P_I(11:18,:);

%Possible 8/12 End
I.pos.haoa = P_I(1:10,:);
```

Analyzing Data Consolidation Methods

```
[r2_1a,r2_1b] = Cav_Ellipse_Exp(I.all.all);
[r2_2a,r2_2b] = Cav_Ellipse_Exp(I.pos.all);
[r2_3a,r2_3b] = Cav_Ellipse_Exp(I.def.all);
[r2_4a,r2_4b] = Cav_Ellipse_Exp(I.all.lre);
[r2_5a,r2_5b] = Cav_Ellipse_Exp(I.all.hre);
[r2_6a,r2_6b] = Cav_Ellipse_Exp(I.all.laoa);
[r2_7a,r2_7b] = Cav_Ellipse_Exp(I.all.haoa);
[r2_8a,r2_8b] = Cav_Ellipse_Exp(I.pos.lre);
[r2_9a,r2_9b] = Cav_Ellipse_Exp(I.pos.hre);
[r2_10a,r2_10b] = Cav_Ellipse_Exp(I.pos.laoa);
[r2_11a,r2_11b] = Cav_Ellipse_Exp(I.pos.haoa);
[r2_12a,r2_12b] = Cav_Ellipse_Exp(I.def.lre);
[r2_13a,r2_13b] = Cav_Ellipse_Exp(I.def.hre);
[r2_14a,r2_14b] = Cav_Ellipse_Exp(I.def.laoa);
[r2_15a,r2_15b] = Cav_Ellipse_Exp(I.def.haoa);
```

```
function [r2_Kmin,r2_Kmax] = Cav_Ellipse_Exp(I)
```

Calculating Transformed Data

```
tran_MI = I(:,4).^2.*I(:,8).^0.4;
```

Creation of Expected Linears

```
x = 0:max(tran_MI)/(length(tran_MI)-1):max(tran_MI);
Exp1 = 0.045*x;
Exp2 = 0.073*x;
```

Calculation of r^2 Values for Expected K Bounds

```
r2_Kmin = 1-sum((I(:,7)'-Exp1).^2)/sum((I(:,7)-mean(I(:,7))).^2);
r2_Kmax = 1-sum((I(:,7)'-Exp2).^2)/sum((I(:,7)-mean(I(:,7))).^2);
```

Plotting Data Against Expected

```
figure
hold on
plot(x,Exp1,'k--','linewidth',2)
plot(x,Exp2,'k:','linewidth',2)
plot(tran_MI,I(:,7),'ko','markerfacecolor','r','markersize',6)
title('Comparison of Data to Expected','fontsize',18)
xlabel('C_L^2Re^{0.4}','fontsize',16)
ylabel('\sigma','fontsize',16)
set(gca,'fontsize',14)
legend('K = 0.045','K = 0.073','Data')
hold off
```

```
end
```

Arndt Expected Relations

```
clear all; close all; clc
data2 = xlsread('Raw Data - General Cavitation','General - Calculated','A3:W82');
data1 = xlsread('Raw Data - End Cap Cavitation','End Cap - Calculations','A3:W82');
data1 = [data1(:,1:3),data1(:,19:23)];
data2 = [data2(:,1:3),data2(:,19:23)];
D_I1 = data1(2:4:end,:);
D_I2 = data2(2:4:end,:);
```

Gathering Desired Data - Definite Cavitation, High Reynolds

```
I_ec = [D_I1(1:2,:);D_I1(6:7,:);D_I1(11:12,:)];
I_g = [D_I2(1:2,:);D_I2(6:7,:);D_I2(11:12,:)];
```

Seperating by speed for Plotting

```
I_ec_700 = I_ec(2:2:end,:);
I_ec_900 = I_ec(1:2:end,:);
I_g_700 = I_g(2:2:end,:);
I_g_900 = I_g(1:2:end,:);
```

Creation of Expected Lines

```
x = 0:10:100;
y1 = 0.043*x;
y2 = 0.075*x;
```

Transforming Data

```
It_ec700 = I_ec_700(:,4).^2.*I_ec_700(:,8).^0.4;
It_ec900 = I_ec_900(:,4).^2.*I_ec_900(:,8).^0.4;
It_g700 = I_g_700(:,4).^2.*I_g_700(:,8).^0.4;
It_g900 = I_g_900(:,4).^2.*I_g_900(:,8).^0.4;
```

Plotting Data

```
figure('color',[1,1,1])
hold on
plot(x,y1,'k--','linewidth',2)
plot(x,y2,'k:','linewidth',2)
plot(It_ec700,I_ec_700(:,7),'ko','markerfacecolor','r')
plot(It_ec900,I_ec_900(:,7),'ko','markerfacecolor','b')
plot(It_g700,I_g_700(:,7),'kv','markerfacecolor','r')
plot(It_g900,I_g_900(:,7),'kv','markerfacecolor','b')
title('Expected Cavitation for Foil With Elliptical Load Distribution: \sigma=KC_L^2Re^{0.4}','fontsize',18)
xlabel('C_L^2Re^{0.4}','fontsize',16)
ylabel('\sigma','fontsize',16)
set(gca,'fontsize',14)
legend('K_m_i_n=0.045','K_m_a_x=0.075',strcat('End Cap: Re~',num2str(round(mean(I_ec_700(:,8)),-
4)/1000),'(10^3)'),strcat('End Cap: Re~',num2str(round(mean(I_ec_900(:,8)),-4)/1000),'(10^3)'),strcat('General:
Re~',num2str(round(mean(I_g_700(:,8)),-4)/1000),'(10^3)'),strcat('General: Re~',num2str(round(mean(I_g_900(:,8)),-
4)/1000),'(10^3)'))
grid on
box on
hold off
```